~~Permafrost thaw couples~~ Thaw-driven mass wasting couples slopes with downstream systems and effects propagate through Arctic drainage networks.

Steven V. Kokelj[1], Justin Kokoszka[1,2], Jurjen van der Sluijs[3], Ashley C.A. Rudy[1], Jo~~h~~n Tunnicliffe[4], Sarah Shakil[5], Suzanne E. Tank[5], Scott Zolkos[5,6]

[1]Northwest Territories Geological Survey, Yellowknife, NT, X1A 2L9, Canada

[2]Wilfrid Laurier University, Yellowknife, NT, X1A 2L9, Canada

[3]Northwest Territories Centre for Geomatics, Yellowknife, NT, X1A 2L9, Canada

[4]~~Department of Earth Sciences~~School of Environment, University of Auckland, Auckland, NZ

[5]Department of Biological Sciences, University of Alberta, Edmonton, AB, T6G 2E3, Canada

[6]Woodwell Climate~~s Hole~~ Research Centre, Falmouth, MA, 02540, USA

Correspondence to: Steven V. Kokelj (steve_kokelj@gov.nt.ca)

Abstract.

The intensification of thaw-driven mass wasting is transforming glacially-conditioned permafrost terrain, coupling slopes with aquatic systems, and triggering a cascade of downstream effects. Within the context of recent, rapidly evolving climate controls on the geomorphology of permafrost terrain, we: (A) quantify three-dimensional slump enlargement and describe the processes and thresholds coupling slopes to downstream systems; (B) investigate catchment-scale patterns of slope thermokarst ~~(thaw slumps and slides)~~ impacts and the geomorphic implications; and (C) ~~project~~ map the propagation of effects through hydrological networks draining ~~continuous~~ permafrost terrain of northwestern Canada. Power-law relationships between thaw-slump area and volume (R^2 = 0.90), and thickness of permafrost thawed (R^2 = 0.63), combined with the multi-decadal (1986~~5~~-2018) increase in areal extent of thaw-slump disturbance, show a two-orders of magnitude increase in catchment-scale geomorphic activity and the coupling of slope and hydrological systems. Predominant ~~catchment~~ effects are to first- and second-order streams where sediment delivery, often indicated by formation of recent debris tongue deposits, commonly exceeds the~~ir~~ transport capacity of headwater streams by orders of magnitude indicating centennial to millennial-scale perturbation of downstream systems. Assessment of hydrological networks indicates thaw-driven mass wasting directly affects over 6,760 km of stream segments, 890 km of coastline and 1,370 lakes in the 994,860 km^2 study area. Downstream propagation of slope thermokarst indicates a potential increase in the number of affected lakes by at least a factor of 4 (n >5,600)~~,~~ and impacted stream length by a factor of 7 (>48,000 km), and defines several major impact zones to lakes, deltas and coastal areas. Prince of Wales Strait is the receiving marine environment for greatly increased sediment and geochemical fluxes from numerous slump impacted hydrological networks draining ~~the landmasses of~~ Banks and Victoria Islands. Peel and Mackenzie Rivers are globally significant conveyors of the slope thermokarst cascade, delivering effects to North America's largest Arctic delta and the Beaufort Sea. Climate-driven erosion of ice-rich slopes in permafrost-preserved glaciated terrain has triggered a time-transient cascade of downstream effects that signal the rejuvenation~~newal~~ of post-glacial landscape evolution. Glacial legacy, ground-ice conditions, and ~~the patterns of continental drainage~~continental drainage patterns dictate that terrestrial, freshwater, coastal, and marine environments of western Arctic Canada will be an interconnected hotspot of thaw-driven change through the coming millennia.

1 Introduction

Climate-induced permafrost thaw will drive the geomorphic evolution of~~ circumpolar~~ circumpolar ice-rich landscapes (Kokelj and Jorgenson, 2013), and ~~t~~terrestrial, freshwater and coastal ecosystems (Vonk et al., 2019). Thawing of ice-rich, glacially-conditioned permafrost terrain (Kokelj et al., 2017a) is rapidly mobilizing vast stores of previously frozen materials, reconfiguring slopes and impacting downstream environments (Fig. 1) (Balser et al., 2014; Rudy et al., 2017a; Tank et al., 2020). These and other similar results highlight the need to quantify slope thermokarst~~slope thermokarst~~ intensification in a robust ~~physical~~geomorphic framework, better understand the rapidly evolving linkages between thawing slopes and downstream environments, and predict the propagation of effects across watershed scales.

The nature of permafrost thaw and downstream consequences will ~~increasingly ~~define trajectories of environmental change in Arctic terrestrial and aquatic systems~~ change~~. Study of thawing slopes and shorelines (Lacelle et al., 2010; Ramage et al., 2017; West and Plug, 2008), and characterization of permafrost physical and geochemical properties (Lacelle et al., 2019), informs the projection of downstream cumulative-effects and implications for carbon and contaminant mobilization (Littlefair et al., 2017; Ramage et al., 2018; St. Pierre et al., 2018; Tank et al., 2020). Recent, rapid increases in the areal extent of upland thermokarst (Lewkowicz and Way, 2019; Segal et al., 2016a; Ward-Jones et al., 2019), and shifts in hydrological, sedimentary and geochemical regimes (Abbott et al., 2015; Kokelj et al., 2013; Littlefair et al., 2017; ~~Malone et al., 2013~~Rudy et al. 2017a) can be linked with significant aquatic ecosystem impacts (Chin et al., 2016; Houben et al., 2016; Levenstein et al., 2018; Thienpont et al., 2013). The processes and feedbacks driving the ~~recent ~~evolution of thawing slopes (Kokelj et al., 2015; Zwieback et al., 2018) ha~~s~~ve received less attention. Thaw-driven landslide effects on permafrost catchments have been investigated through nested watershed studies (Beel et al., 2018; Bowden et al., 2008; Shakil et al., 2020a; Zolkos et al., ~~in review~~2020), and the cascade of effects have been inferred through geochemical trend analyses of large Arctic rivers (Tank et al., 2016; Zolkos et al., 2018). The broad-scale distribution of slope thermokarst determined through empirical (Kokelj et al., 2017a), remote sensing (Brooker et al., 2014; Nitze et al., 2018), GIS mapping~~;~~ (Olefeldt et al., 2016), and modelling approaches (Rudy et al., 2017b) have typically not been designed to elucidate physical processes, downstream connectivity, and attendant effects. Despite the growing geomorphic and geochemical influence of thaw-driven mass wasting on terrestrial, aquatic, and marine systems (Vonk et al., 2019), and the potential for rapid carbon release

(Turetsky et al., 2020), fundamental knowledge gaps persist in our understanding of climate-driven amplification of slope thermokarst, the evolution of downstream linkages and the cascade of consequences.

Retrogressive thaw-slumps, complex thaw-flow slides, and shallow and deep translational failures are amongst the most dynamic forms of slope thermokarst (Alysworth, 2000; Kokelj et al., 2015; Rudy et al., 2017b). Anticipating the cumulative effects of ~~slope thermokarst~~thaw-driven mass wasting ~~intensification~~ on permafrost landscapes and downstream environments requires a better knowledge of ~~thaw-driven geomorphic~~ processes and the evolution of connectivity across a range of spatial scales. First, exploring the ~~geomorphic and geochemical~~ implications of ~~slope disturbance~~thaw-driven mass wasting requires determining the relationships between disturbance area, volume, and ~~depth~~ thickness of permafrost thawed so that changes in landslide count or areal extent (Lantz and Kokelj, 2008; Lewkowicz and Way, 2019; Ward-Jones et al., 2019) can be considered in a more robust physical framework (van der Sluijs et al., 2018). To advance understanding of processes and feedbacks driving the ~~rapid~~ evolution of slope thermokarst ~~disturbance~~ and hillslope-~~-~~channel coupling, ~~including the patterns and rates of thaw-driven disturbance enlargement, downslope transport of material derived from erosional features, and quantification of slope sediment budgets,~~ conventional satellite- and airborne-derived planform ~~information on slope mass-wastin~~terrain assessments~~g~~ should be quantified with high-resolution 3D survey techniques~~, such as Light Detection and Ranging (LiDAR), or drone-based Structure-from-Motion (SfM).~~. Secondly, ~~analysing~~ analyzing thermokarst mass-wasting effects within ~~the context of~~ a hydrological ~~drainage~~ network context is required to ~~advance the understanding of~~understand slope-to-stream linkages and downstream connectivity (Wohl et al., 2019), and to provide a platform for description and modelling ~~. Describing slope thermokarst within a hydrological framework will enable the description~~ of watershed effects~~, and provide a platform for modelling the transient propagation of geomorphic and geochemical impacts~~. Finally, considering ~~thermokarst~~ the distribution of thermokarst mass-wasting processes and trajectories of change within an appropriate theoretical or geomorphic ~~context~~ context (Ballantyne, 2002) will support the explanation of spatial patterns, rates and magnitudes of geomorphic change (Kokelj et al., 2017a), and geochemical effects (Lacelle et al., 2019; Tank et al., 2020), and ~~the contextualization of~~contextualize ~~thermokarst field investigations, as well as~~ conceptual and physically-based models (Turetsky et al., 2020).

~~To address these knowledge gaps, and specifically, to better understand the~~ The goals of this study are to better understand (A) the geomorphic ~~processes that drive the intensification of~~changes that result from thaw-driven mass wasting and the evolution of slope to stream coupling, (B) the spatial distribution of catchment effects, and (C) their propagation across watershed scales. Here~~,~~ we present a suite of spatially nested case-studies bounded by Arctic drainage from permafrost terrain ~~from continuous permafrost~~ of northwestern Canada (Fig. 1). The study area is predominantly in the zone of continuous permafrost however, we also include the Great Bear River drainage and a few other Mackenzie River tributaries that drain northern margins of the extensive discontinuous permafrost zone. This 10^6 km^2 study region contains a wide range of climate and permafrost temperature regimes (Smith et al., 2010), ground ice conditions (O'Neill et al., 2019), biophysical gradients (Lantz et al., 2010), and geological environments, including unglaciated and glaciated terrain (Dyke and Prest, 1987; Dyke et al., 2003). The latter is of central relevance to study design, in particular where permafrost has maintained ice-marginal moraine, glaciolacustrine, glaciofluvial, and glaciomarine deposits in a quasi-stable state, preserving relict ground ice (Lakeman and England, 2012; Mackay, 1971; Murton et al., 2005; Pollard, 2000) and constraining slope evolution through a cooling Holocene climate (Porter et al., 2019). Today, these environments host ~~numerous~~ large areas affected by~~of~~ intense thaw-driven geomorphic change (Fig. 1) where landslides, predominantly in the form of retrogressive thaw slumps, or retrogressive thaw-flow slides, are mobilizing slope materials, transforming landscapes (Kokelj et al., 2015), and triggering an array of downstream effects (Chipman et al., 2016; Rudy et al., 2017a; Zolkos et al., 2018). ~~The focus of~~The fine-scale investigations in this ~~study~~research ~~mainly considered~~focused on retrogressive thaw slumping because it is a primary mode of thaw-driven slope failure in the study region (Segal et al., 2016a), and ~~often a modifier of~~it can modify slopes affected by other~~subject to other types of~~ landslides types. ~~Our b~~Broad-scale mapping to address goal (C) ~~included~~ considered multiple slope failure modes (~~, including~~ thaw slumps,~~ and~~ shallow and deep translational slides), so we utilized more inclusive terminology such as slope thermokarst, ~~slope thermokarst, or~~ thaw-driven landslides, or~~and~~ mass wasting when discussing these results.

To quantify the enlargement ~~rates~~ of retrogressive thaw slumps, assess allometric relationships (i.e. area and volume) (cf. Bull, 1964), and to explore thresholds that govern slope-to-stream connectivity (~~Objective~~ goal A), we ~~analysed~~ analyzed fine-scale topographic data derived from LiDAR for a large population of thaw slumps from across ~~biophysical transitions on~~ the Peel Plateau (Kokelj et al., 2017b), and a second population within the Anderson Plain and Tuktoyaktuk Coastlands areas (Rampton, 1988), and from repeat Unmanned Aerial Vehicle (UAV) terrain surveys of individual disturbances on the Peel Plateau (Fig. 1, Table S1). To investigate thermokarst mass-wasting effects on catchments~~-scale patterns of slope thermokarst effects~~ (~~Objective~~ goal B), we combined thaw-slump mapping with empirical models to estimate disturbance volume, to visualize the~~assess~~ patterns and intensity of impacts across a fluvial network,~~fluvial patterns of thermokarst effects~~ and to derive first-order estimates of slope denudation for a medium-sized catchment (Willow River, 10^3 km^2) in the Mackenzie Delta region (Fig. 1, Table S1). Detailed investigations of the distribution of ~~slope~~ thermokarst mass wasting ~~disturbance~~ ~~distribution~~ within a fluvial network were extended to a range of catchment~~t scale~~s for the northern Peel Plateau (3,520 km^2) and ~~compared with conditions from~~ southeastern Banks Island (1,220 km^2), and patterns of fluvial-geomorphic effects were explored by contrasting stream sediment fluxes across catchment scale and disturbance status. To assess the potential propagation of ~~slope thermokarst across broad spatial scale~~watershed-scale slope thermokarst effects (10^4 to 10^5 km^2) ~~s~~ (~~Objective~~ goal C), disturbance distribution ~~watershed-scale assessments (10^4 to 10^5 km^2) of slope thermokarst effects were~~was ~~analysed~~ analyzed within a Strahler-order framework for composite drainage areas characterized by contrasting terrain and permafrost conditions that we defined for this study as the Banks Island, Amundson Gulf, Peel River and Keele-~~/~~Redstone watersheds (Fig. 1, Table S1). Finally, ~~slope thermokarst~~thaw-driven mass wasting effects on stream, lake, and coastal environments were integrated through a flow accumulation analysis to ~~project~~ map the potential cascade of

~~thermokarst~~ effects through hydrological networks of northwestern Canada (Fig. 1). Through this multi-scale study, we~~With these data and analyses, we~~ link the intensification of thaw-driven slope processes with the coupling of downstream systems and map the propagation of effects through hydrological networks, showing ~~to show~~ the interconnected nature of slope thermokarst hotspots~~,~~ and ~~to project~~ the patterns of emerging sedimentary and geochemical regimes that will define major Arctic change through the coming millennia.

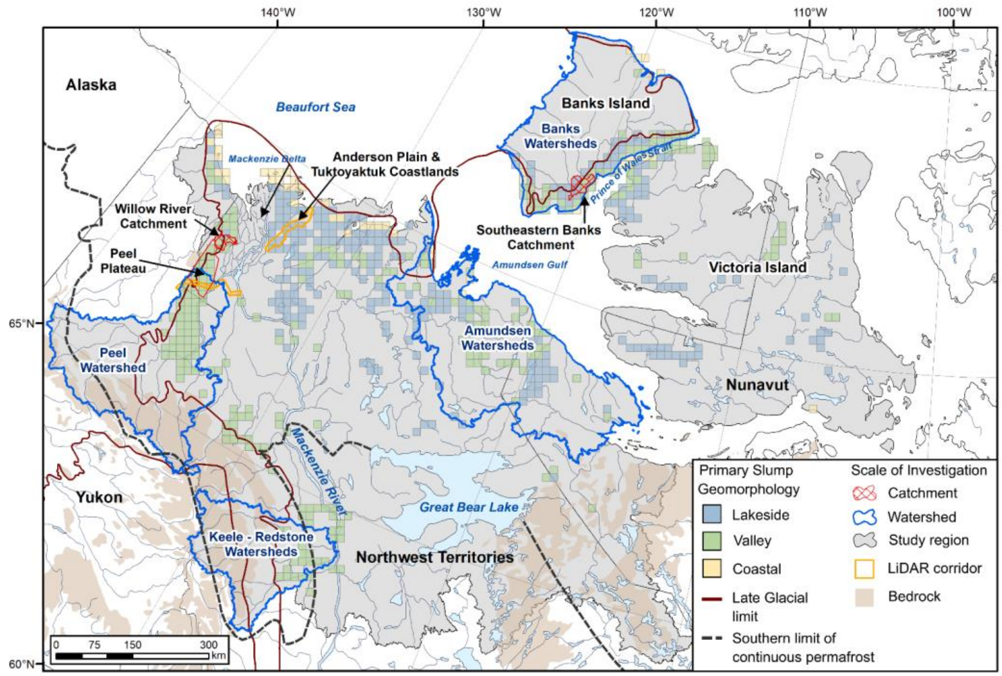

140°W
130°W
120°W
110°W
100°W
65°N
60°N
Alaska
Beaufort Sea
Banks Island
Banks Watersheds
Mackenzie Delta
Anderson Plain & Tuktoyaktuk Coastlands
Willow River Catchment
Peel Plateau
Prince of Wales Strait
Southeastern Banks Catchment
Amundsen Gulf
Victoria Island
Amundsen Watersheds
Peel Watershed
Nunavut
Mackenzie River
Yukon
Great Bear Lake
Keele - Redstone Watersheds
Northwest Territories
0 75 150 300 km
Primary Slump Geomorphology
Lakeside
Valley
Coastal
Late Glacial limit
Southern limit of continuous permafrost
Scale of Investigation
Catchment
Watershed
Study region
LiDAR corridor
Bedrock

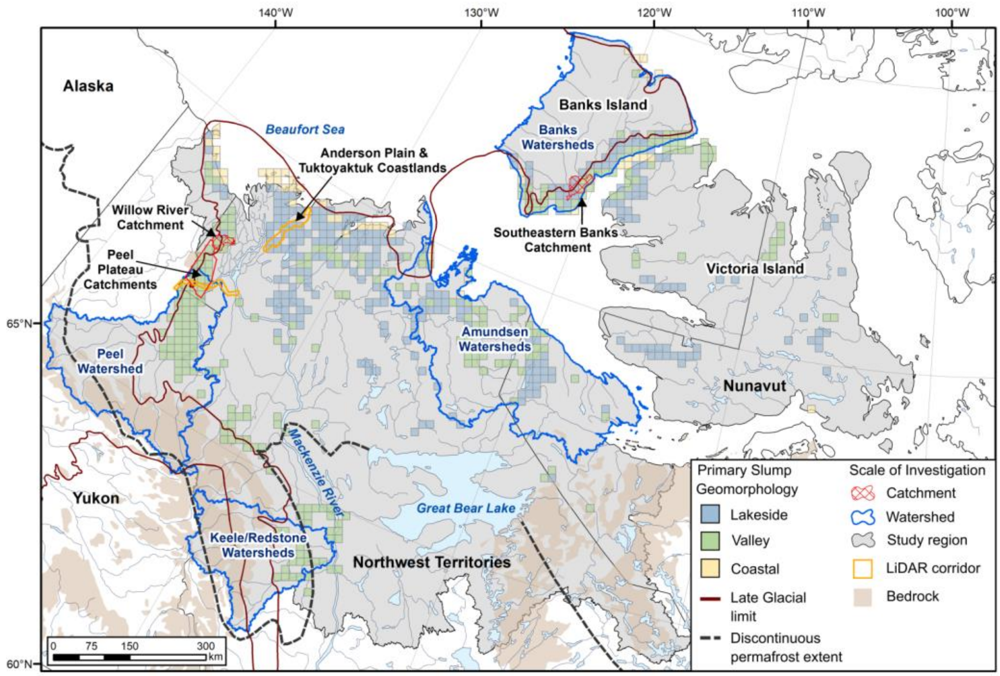

Figure.1. Study region map showing the distribution and dominant geomorphic environments affected by thaw-driven mass wasting, and the locations and scales of investigation constrained by the 994,860 km^2 area of Arctic drainage from permafrost terrain of ~~continuous permafrost of~~ northwestern Canada. Fine-scale thaw slump mapping utilizing ~~high~~ high-resolution UAV and LiDAR terrain models is indicated by the orange corridors (Peel Plateau; ~~and~~ Tuktoyaktuk Coastlands and Anderson Plain); small to medium scale catchments including Willow River, Peel Plateau and southeastern Banks Island areas are indicated by red polygons; ~~major~~ focal watersheds are outlined in blue, and the Arctic drainage study area~~from continuous permafrost which defines the broadest scale of investigation~~ is shaded in grey. The disturbance data on the map ~~is~~ are adapted from Segal et al., 2016b and Kokelj et al., 2017a. L~~L~~ate glacial limit is from Dyke and Prest, 1987, bedrock geology is from Fulton, 1995, and the permafrost boundary is from Brown et al., 1997. The Willow River Catchment is part of a sub-sub-drainage, and the Watershed~~,~~ and Study area boundaries are composites of several sub-sub-drainage areas (Method S1-3) from the National Hydro Network (NHN) geodatabase (Natural Resources Canada, 2016). ~~Base~~ The base map is from ESRI ArcGIS Online.

2 Study area and methods

Formatted: None, Space Before: 0 pt, After: 0 pt, Line spacing: 1.5 lines, Don't keep with next

2.1 Study Area

This broadest scale of inquiry is defined as the Arctic drainage networks of northwestern Canada, primarily from continuous permafrost and the northern limits of extensive discontinuous permafrost terrain ~~Arctic drainage from continuous permafrost of northwestern Canada~~(Fig. 1). The ~~comprises an area of about 1 million~~994,860 km^2 Arctic drainage area of northwestern Canada is comprised of 68 sub-sub-drainage areas from the National Hydro Network geodatabase (Method S2) (Natural Resources Canada, 2016). This study area is ~~, characterized by diverse permafrost~~characterized by a diversity of~~,~~ permafrost, geological, climate, and ecosystem conditions (Fig. 1). The Mackenzie and Peel River systems drain the ~~south~~ south-central and western parts of the study area. Several small hydrological systems characterize the Yukon Coastal plain, whereas ~~middle~~ medium to large ~~northward~~ northward-flowing rivers drain tundra of the interior platform and shield terrain northeast of the Mackenzie Basin. An abundance of small to ~~medium~~ medium-sized streams comprise~~s~~ the tundra watersheds of Banks and Victoria Islands.

~~This large~~The study area ~~includes~~ is characterized by forested and alpine tundra ~~warm permafrost~~ in the southern and western regions where mean annual ~~ground~~ temperatures at the top of permafrost (TTOP) in undisturbed terrain ~~in undisturbed forested and alpine tundra terrain~~ range from above -1°C to about -3°C (Smith et al., 2010; O'Neill et al., 2015), a transition to low Arctic tundra where permafrost is typically greater than 100 m in thickness with mean annual TTOP~~nnual ground temperatures~~ below -4°C (Kokelj et al., 2017c), and Arctic tundra of Banks and Victoria Islands where frozen ground is hundreds of metres thick and mean annual TTOP is typically below -10°C (Smith et al., 2010). Abundant ice-rich terrain in the region is indicated by the widespread occurrence of segregated, wedge, and ~~ice,~~ relict ground ice~~, and ice-wedge ice,~~ (O'Neill et al., 2019 and references within). The distribution and abundance of these main ground-ice types are associated with the legacy of glaciation, distribution of fine-grained, frost-susceptible sediments, and a cold Holocene climate. The spatial distribution of retrogressive thaw slumps ~~in this region~~ confirms the abundance of ice-rich terrain and ~~thaw~~ thaw-sensitive slopes~~,~~ and the broad-scale association with ice-marginal, permafrost preserved glacigenic terrain (Fig. 1) (Kokelj et al., 2017a). The unglaciated western margins of the study region are mountainous, and permafrost is generally ice-poor. Numerous ~~high~~ high-energy streams and rivers draining the Cordillera have incised ~~ice-rich~~ unconsolidated, ice-rich glacial deposits along their course to the Mackenzie or Peel Rivers. These thick deposits of fine-grained tills and other glacigenic materials, derived primarily from sedimentary bedrock, define the western margins of the Laurentide glacial limits and ~~the~~ contrast with the eastern ~~part of the~~ part of the study region~~, which is~~ characterized by ~~extensive areas of~~ shield bedrock veneered by patches of glacial materials derived from Precambrian rock (Dyke and Prest, 1987). The predominant form of slope ~~slope~~ thermokarst mass-wasting across the region is retrogressive thaw slumps (Kokelj et al., 2017a), with shallow ~~landslides~~ and deep-~~-~~seated landslides~~translational failures~~ having local importance that increases southward, particularly in areas of greater relief (Aylsworth et al., 2000). To examine the processes driving the intensification of ~~slope thermokarst~~thaw-driven mass wasting and the patterns of effects across hydrological networks, we applied multiple methods involving field study and mapping at slope, catchment, and watershed scales described in the following sections~~. Datasets supporting this work~~ and summarized in Table S1~~ include (Kokoszka and Kokelj, 2020; Rudy and Kokelj, 2020; Rudy et al., 2020; Shakil et al., 2020b)~~.

2.2 Fine-scale topographic data to explore hillslope-channel coupling

To describe ~~slope-scale pr~~processes of thaw slump development and slope-to-stream connectivity, terrain surveys by airborne LiDAR from fixed-wing aircraft and structure from motion (SfM) photogrammetry from UAV were used to derive a sequence of Digital Terrain Models (DTMs) (van der Sluijs et al., 2018) covering an 8-year span from 2011 to 2018. These surveys comprised a series of ~~repeat~~ DTMs enabling total and annual volumes of material displaced by thaw-driven mass wasting to be estimated by~~:~~ 1) calculating differenced DTMs (DOD); 2) determining uncertainties and masking DODs based on minimum levels of change detection thresholds; and 3) summarizing the ~~cell~~ values for the scar-zone (erosion) and debris tongue (deposition). Full data acquisition and processing methods are provided in van der Sluijs et al (2018). Survey metadata are~~is~~ provided in Table S~~1~~2.

Overlapping UAV photos were acquired from a size continuum of slump~~-feature~~s ~~of varying sizes~~ on the Peel Plateau (Fig. 1) between 2015 and 2018, along with ground control data acquired through differential Global Navigation Satellite System (GNSS) surveys. Aerial photo datasets were processed into georeferenced colour orthomosaics and point clouds using SfM software packages (Smith et al., 2016). Noise-filtered and ground-classified point clouds were ~~rasterised~~ rasterized in 0.5-m spatial resolution bare-earth DTMs and resampled bilinearly to 1 ~~-~~m spatial resolution for spatial consistency with LiDAR models. The LiDAR data with an average point density of 1.7 m^{-2} was collected on 25-28 August 2011 by vendor McElhanney Consulting Services Ltd. (Vancouver, BC, Canada) along two study corridors (Fig. 1). The first is a 162 ~~-~~km long, 6 to ~~-~~9 ~~-~~km ~~-~~wide portion of the Dempster Highway across the Peel Plateau comprising an area of 1,032 km^2 (O'Neill et al., 2015; Kokelj et al., 2017b). The second corridor is a 9 to ~~-~~19 ~~-~~km wide and 139 ~~-~~km long area (1,478 km^2)~~,~~ comprising the Inuvik-to-Tuktoyaktuk Highway corridor which crosses the Anderson Plain and Tuktoyaktuk Coastlands (Rampton, 1988). Following initial processing by the vendor, a baseline 1-m LiDAR DTM was created in ESRI ArcGIS 10.4.1 ("LAS Dataset to Raster" tool) using mean ground point elevations and Delaunay triangulation with linear interpolation to fill data voids. Vertical datum differences between the LiDAR and UAV surveys were corrected to ensure data compatibility.

To explore the associations between thaw slump enlargement and slope-to-stream coupling, we quantified the volumes of slump erosional concavities and debris tongue deposits for a ~~slump~~ size-age continuum exemplified in five disturbances in the Peel Plateau region where DTM data was derived from 2018 UAV surveys (Table S2). Notably, geomorphic activity at one of the thaw slumps (CB) had accelerated significantly throughout the monitoring record (2011-2018)~~ (Table S1)~~. The 2011 LiDAR DTM provided a topographic baseline that could be used to reconstruct pre-disturbance terrain surfaces so that volumetric changes associated with thaw-driven subsidence, and ~~thaw-driven~~ slope erosion~~,~~ and downstream deposition could be estimated. The pre-disturbance surfaces were manually reconstructed using LiDAR-derived 2-m contours aided by historical aerial photographs, and circa 1970 Canadian Digital Elevation Model (CDEM) (~~Government of Canada, 2000~~Natural Resources Canada, 2015), following van der Sluijs et al. (2018). Pre-disturbance valley morphology required valley-bottom elevations to be constrained, so undisturbed stream elevations were sampled at 10-~~ ~~m intervals along transects that extended up to~~up to~~ 200 m ~~above and below~~beyond the upper and lower limits of the debris tongue deposits. Fitted polynomial curves were used to model pre-disturbance valley bottoms, constraining contour line reconstructions, which were interpolated to a 1-m DTM using the ArcGIS 10.4.1 "Topo-to-Raster" tool. Total scar zone and debris tongue volumes were estimated, and DODs provided a volumetric estimate of the year~~ to ~~-to-year changes.

2.3 Regional Scale Data Acquisition and Processing

To explore relationships between planform thaw slump scar area and ~~volumetric erosion~~volume, we digitized scar areas~~,~~ and estimated the volume and depth of the ~~erosional~~ disturbance concavities for a subsample of 71 thaw slumps from the 2011 LiDAR corridors described ~~above~~ in Sect. 2.2 and shown on Figure~~(Fig.~~ 1~~)~~. Features were digitized by J. van der Sluijs and reviewed for accuracy and consistency by SV Kokelj (Table S1). Utilizing LiDAR hill-~~-~~shaded DTMs and ~~optical airborne~~airborne optical imagery (2011-2012), all active or recently-active scar and debris tongue areas determined by a distinct scarp and bare or sparsely vegetated scar area were digitized at a 1:2,000 scale. Each polygon defined either a scar zone where the debris tongue was indistinguishable or a scar-only area where a debris tongue could be identified as a geomorphic feature distinct from the active scar zone. Slumps were designated as being associated with fluvial, lacustrine, or coastal systems, with an assigned integer to indicate the downstream connectivity, where "0" is no connection with the downstream environment; "1" is connection between the bare scar area and downstream environment, and "2" indicates evidence of downstream deposition, which is expressed as a~~, including a~~ debris tongue in a valley bottom, or a sediment lobe protruding into an adjacent lake or coastline.

For developing regional-scale slump DTMs and DODs, we followed general procedures described in Sect. 2.2, with some adaptations to streamline processing of a large sample population. Firstly, only "classic" cuspate or ~~bowl~~ bowl-shaped thaw slump forms were assessed~~targeted for analysis~~: more complex elongated and polycyclic features, common along shorelines, introduced greater uncertainty in the process of automated pre-disturbance terrain reconstruction. Several parameter adjustments in ArcGIS LAS Dataset to Raster tool were implemented to minimize vegetation influences. Rather than linearly triangulating mean elevation of ground-classified points, minimums were binned into a 1-m grid to better represent ground elevation in (re-)vegetated terrain (Gould et al., 2013; Meng et al., 2010). Reconstructing pre-disturbance slump topography was automated by removing all points in the slump scar and interpolating the pre-disturbance surface with points adjacent to the scar. Natural neighbour void-filling interpolation was applied as a balance between accuracy and shape reliability across a range of natural environments (Bater and Coops 2009; Boreggio et al., 2018). The 2011 LiDAR and derived pre-disturbance DTMs were differenced into a DOD, and results were summarized with the ArcGIS "Zonal Statistics" tool.

2.4 Catchment scale mapping and analyses of sediment flux

To examine ~~fine-scale~~ the patterns of thaw-slump occurrence within a drainage network, slope to stream ~~, network~~ connectivity, and changes ~~in these parameters~~ through time, we investigated the 80~~0~~6 km² W~~W~~illow River catchment on Peel Plateau ~~(Fig. 1)~~ because ~~the fluvially-incised stream~~ it~~network~~ straddles the late Wisconsinan glacial limit, and much of the fluvially-incised basin is intensely affected by thaw slumping (Fig. 1) (Lacelle et al., 2010). To examine temporal change~~, in this catchment~~ we created digitized inventories of active thaw slumps from the Willow River catchment utilizing cloud-free Landsat imagery from 1986, 2002 and 2018 (Table S1)~~described in~~ (Rudy and Kokelj, ~~(~~ 2020). To further explore catchment-scale patterns of slope disturbances over ~~larger areas~~multiple watersheds in different regions~~, and potential contrasts between ice-rich glacigenic study regions~~, and potential changes in these patterns through time, we used 2016-2017 Sentinel-2 imagery to re-assess the 2005~~4~~-2010~~05~~ slump mapping determined using SPOT 4/5 satellite imagery (Segal et al., 2016c, d) for a 3,520 km² area of the northern Peel Plateau and 1,220 km² of southeastern Banks Island (Fig. 1) (Rudy et al., 2020). To assess the distribution of thaw slumps within a catchment framework, w~~Catchment areas upstream of thaw slumps were estimated using~~ e used CDEM, and applied~~.~~ Tau-DEM (v.5.3) "Fill", "D8", and "Flow Accumulation" algorithms (http://hydrology.usu.edu/taudem/) (Tarboton, 1997)~~were applied~~ to trace the drainage networks and determine ~~upstream~~ the ~~catchment areas~~upstream contributing area for each thaw slump.

Formatted: Not Highlight

Formatted: Not Highlight

Sediment fluxes for Peel Plateau streams draining glaciated and unglaciated terrain were calculated to assess effects of catchment size and thermokarst disturbance (Shakil et al., 2020b). Instantaneous total suspended sediment (TSS) fluxes (mg km^{-2} s^{-1}) were compiled from sampling during the summer flow period (July – September) for 2010 and~~,~~ 2015-2017. Sampling procedures and catchment delineations are elaborated in Chin et al., 2016 and Shakil et al., 2020a. Historical TSS yields also constrained to July 1st – September 14th were obtained for the Peel River at Fort McPherson (Water Survey of Canada, station 10MC002)~~,~~ by pairing TSS spot sampling with discharge and normalizing to a 70,5~~6~~0~~0~~6 km² watershed area.

2.5 The influence of thaw-driven mass wasting on drainage from ~~continuous~~ permafrost terrain of northwestern Canada

Here we summarize methods to identify individual segments of the hydrological network affected by active thaw-driven mass wasting and the framework to map the ~~potential~~ propagation pathways of ~~slope thermokarst~~ effects through watersheds for Arctic drainage from permafrost terrain of ~~continuous permafrost of~~ northwestern Canada (Fig. 1). Geoprocessing steps are in Supplementary methods 1-3, and the mapping procedure and raw data are in Kokoszka and Kokelj (2021~~0~~). In summary, we used georeferenced, 10m resolution SPOT 4/5 (200~~4~~5-2010) (NWT Centre for Geomatics, 2013) and Sentinel-2 (2016-2017) orthomosaics to identify hydrological segments affected by ~~slope thermokarst~~ mass wasting features for individual stream network, lake, and coastline segments from the 1:50,000 National Hydro Network (NHN) dataset (Natural Resources Canada, 2016) using ArcMap 10.6. The~~The~~ Arctic drainage study area contains 68 NHN Work Units (~~subcatchments~~sub-sub-catchments). The NHN Primary Directed Network Linear Flow (PDNLF) Shapefiles include primary (main route) stream segments and polylines through lakes, and the NHN Waterbody and Littoral Shapefiles represent lakes and coastlines, respectively. Th~~is~~is dataset was combined to define the entire NHN hydrological network for the 994,860 km² drainage area (Fig.~~ure~~ 1).

Formatted: Not Highlight

A 7.5×~~x~~7.5-~~-~~km grid system guided the systematic inventory of ~~slope thermokarst~~thermokarst-~~-~~affected hydrological segments in each of the 68 NHN work units (Kokoszka and Kokelj, 2020). NHN hydrological features were designated as 'directly affected' where one or more ~~active slope-thermokarst features~~active slope thermokarst disturbances were in contact with~~,~~ or exhibited clear drainage towards the hydrological feature. PDNLF features directly influenced by thaw-driven mass wasting~~slope thermokarst~~ were assigned a numeric value of '1'. To enable propagation of effects from lakes, PDNLF features at the lake outflow within directly affected lakes were also assigned a numeric value '1'. Unaffected PDNLF features were assigned a numeric value '0' to indicate no thermokarst effect. All mapping was reviewed for accuracy and consistency (Kokoszka and Kokelj, 2021).

The potential for downstream propagation of ~~slope thermokarst~~slope thermokarst effects was determined by generating a network for each of the 68 Work Units using RivEX 10.25 (Hornby, 2017). A river network was constructed for each PDNLF dataset based on the topology of the original NHN data, where the digitized direction corresponded with flow direction. PDNLF features directly affected by one or more slope-thermokarst features were assigned a value of '1' as indicated above. The "~~'~~Accumulate Attribute Tool"~~'~~ in RivEX 10.25 was used to sum the number of all upstream slope thermokarst affected segments and tabulate this~~d~~ for each Work Unit. One 800 km² catchment (Willow River, see Fig. 1), ~~representing~~ which is part of an NHN Work Unit and comprises a small subset of the total stream network was subjected to additional analysis since detailed thaw-slump mapping (Rudy et al.~~and Kokelj~~, 2020) was available. The total area of mapped thaw slumps and slides for each hydrological segment was summed and accumulated downstream to portray catchment-scale variation in the intensity of disturbance effects (~~Supplementary~~ Method~~s~~ S1).

Formatted: Not Highlight

For the broad and fine-scale analyses, the accumulated count of impacted stream segments was used to identify the longitudinal trace of ~~thermokarst~~ mass wasting effects within each Work Unit (~~Supplementary~~ Method~~s~~ S2). Stream features with an accumulation value > 0 represented the potential propagation pathway of effects through the network. Propagation of effects across watershed scales involved transferring accumulation values from upstream to downstream Work Units. Hydrological features that were influenced by the downstream propagation of slope-~~-~~thermokarst effects were identified as indirectly affected PDNLF features with an accumulation value > 0 and a numeric value of 0. PDNLF features contained within lakes with an accumulation value > 0 indicated indirectly affected lakes, although these lakes could also be attributed as directly affected if the shoreline hosted slope thermokarst features. Coastal segments adjacent to accumulated PDNLF features where streams discharge to the ocean were identified as indirectly affected coastline. After all Work Units were processed, the data were merged to produce a downstream trace with upstream accumulation values for the entire 994,860 km^2 drainage area.

To summarize information on the distribution of watershed effects, Strahler Order was computed (~~Supplementary~~ Method~~s~~ S3) for the 4 major watershed-scale study ~~-~~areas of Banks Island (70,794 km^2), Amundsen Gulf (90,288 km^2), Peel River (76,506 km^2), and Keele-~~/~~Redstone (39,957 km^2) (Fig. 1). For each of the major watersheds, the respective Work Units (sub-sub-drainage areas) and PDNLF Shapefiles were merged, and the 'Strahler Order Tool' in RivEx 10.25 was used to compute Strahler Order for each PDNLF polyline. For each major watershed study area~~sub-basin~~, directly and indirectly, affected streams and lakes were summarized by Strahler Order.

We summarized the total length of thermokarst-affected stream networks and the coastal margins, as well as the total number of ~~thermokarst-~~ thermokarst-affected lakes, including lakes influenced by the downstream propagation of ~~slope-thermokarst effe~~disturbance effects. Mid-points of the directly affected stream, lake, and coastal segments were synthesized in ArcGIS to create a kernel density map~~ portraying the distribution and density of thaw-driven mass wasting effects on hydrological segments across the study area~~. The routing of thermokarst effects was~~ere~~ portrayed through the downstream trace and accumulation values at the coastline to provide a relative estimate of the magnitude of upstream effects~~ at the point where hydrological networks discharge to the ocean~~.~~.~~ This current method does not account for variation in transport gradients, catchment sinks, nor intensity of each disturbance, and therefore represents a semi-quantitative, time-transient snapshot of thaw-driven ~~thaw-driven~~ mass wasting effects on drainage from ~~continuous~~ permafrost terrain of northwestern Canada.

2.6 Statistical analyses

The software package SPSS Statistics 21 (IBM) was used for data exploration, deriving summary statistics, testing inferential qualities, and regression analyses for all LiDAR and ~~UAV-~~ UAV-derived datasets presented in this study. All summary statistics are provided in tabular format in the body of the manuscript or Supplementary materials. Thaw-slump area, volume, and maximum depth of disturbance concavity did not meet assumptions of normality and were logarithmically transformed prior to performing ~~a~~ t-tests to assess differences in slump size ~~indices~~ metrics between physiographic regions, and a one-way analysis of variance and a Tukey's HSD post-hoc test to assess differences across categories describing downstream connectivity. Regression analyses between thaw-slump area and disturbance volume, and thaw-slump area and maximum concavity depth~~,~~ were also performed on the logarithmically transformed datasets. Regression diagnostics included testing the normality of residuals~~,~~ and Cook's distance to test for the presence of unduly influential points.

Additional statistical analyses assessing thaw-driven ~~slope thermokarst~~landslides~~ conditions~~ in the Willow River catchment and potential changes through time were performed in RStudio (Version 1.1.463) using the “stats”, and “FSA” packages (R Core Team, 2017). In this case study, non-parametric statistical testing (Kruskall-Wallis and Dunn’s post-hoc tests) was implemented to assess potential differences in slump size indices between three~~3~~ different time periods.

3 Results

Here we document: (A) the rapid evolution of thaw-driven mass ~~-~~wasting and slope-to-stream coupling, (B) the spatial patterns of thermokarst effects within catchments, and (C) their propagation through hydrological networks and across watershed scales. The first three subsections focus on slope-scale processes with emphasis on the thresholds that have transformed connectivity between ~~thawing slopes~~thaw-driven mass wasting and downstream systems (3.1, 3.2), and the scaling of thaw-slump dimensions associated with areal enlargement (3.3). The fourth and fifth subsections (3.4, 3.5) focus on quantifying the changing patterns and magnitudes of thermokarst and the potential downstream effects within hydrological networks up to the medium catchment (10^4 km^2) scale. The final subsection (3.6) provides flow accumulation analysis results ~~to~~ that explore~~ the~~ patterns and ~~to~~ project the routing of ~~slope~~ thermokarst mass wasting effects through Arctic drainage networks from~~ continuous~~ permafrost terrain of northwestern Canada.

3.1 Thaw slump intensification transforms slope-to-stream connectivity

To investigate geomorphic change~~sediment transfer~~ associated with ~~intensifying slope thermokarst~~thaw slump enlargement and the evolution of ~~ving~~ linkages between thawing slopes and downslope environments, we used UAV-derived ~~survey~~ elevation data from 2018 to quantify thaw slump and debris tongue volumes for a size and age ~~slump~~ disturbance continuum on the Peel Plateau (Tables 1, S~~1~~2; Figs. 2, S1). The smallest slump (slump D1), which was about a decade old, had an area of 2.8 x 10^3 m^2, ~~an eroded~~a displaced volume of 4.6 x 10^3 m^3, and no debris tongue accumulation (Table 1; Figs. 2a, g). The second-largest feature (slump CB), which initiated around 2002-2004, had accelerated ~~recently accelerated~~ growth through our monitoring period, displaced~~, displacing~~ 1.36 x 10^5 m^3, ~~-~~and formed~~ing~~ a debris tongue that comprised~~ing~~ 20% of the scar volume (Table 1; Figs~~s~~. 2be, ~~hg; Table 1~~, 3)~~. The geomorphic acceleration of slump CB occurred through our monitoring period and is addressed in Sect. 3.2.~~ Over ~~2~~ two decades, two larger slumps, FM3 and Husky, displaced 5.0 x 10^5 m^3 and 6.9 x 10^5 m^3 of material producing debris tongues of 1.5 x 10^5 m^3 and 3.7 x 10^5 m^3, respectively (Table 1). The valley-fills exceed 15 m thickness and approach 1000~~ 1 k~~ m length (Fig. 2g~~h~~), comprising about 30% (FM3) and 50% (Husky) of the estimated scar cavity volumes (Table 1). At Husky slump, the debris tongue raised the base-level of the ~~master (trunk)~~trunk stream, elevating and laterally displacing the stream channel against the side of the valley, causing~~ slope~~ slope erosion and secondary slump initiation (Fig. 2c). Growth~~Enlargement~~ of the Husky slump led to the breaching and rapid lake drainage~~ of a lake~~ in 2015, which flushed scar ~~scar zone~~ colluvium~~materials~~ down valley (Video S1).

Table 1. Scar and debris tongue areas and volumes (sediment erosion and thaw subsidence vs. ~~erosional/~~depositional~~al~~) and debris tongue ~~age~~ age for a slump ~~-~~size-age continuum from September 2018 field observations.

Slump	Location	Tongue ~~Age~~accumulation (yrs.)	Scar Area (m^2)	Scar Volume (m^3)	Debris Tongue Area (m^2)	Debris Tongue Volume (m^3)
D1	67.1771° N -135.7555° W	n/a	2,853	-4,565	Not present	Not present
CB	67.1814° N -135.7295° W	<5	34,084	-136,496	12,007	21,567
FM3	67.2539° N -135.2732° W	>10	73,518	-501,916	31,799	147,025
Husky	67.5207 ° N -135.3005 W	>10	64,386	-690,687	73,696	377,666
FM2	67.2545° N -135.2286° W	>30	337,901	-6,003,927	179,000	1,949,711

Note: Terrain models and delineations of these disturbances are shown in Figure S1.

Formatted: Font: Not Bold
Formatted: Font: Not Bold
Formatted: Centered
Formatted: Centered
Formatted: Centered
Formatted: Centered
Formatted: Centered
Formatted: Centered
Formatted: Font: 8 pt

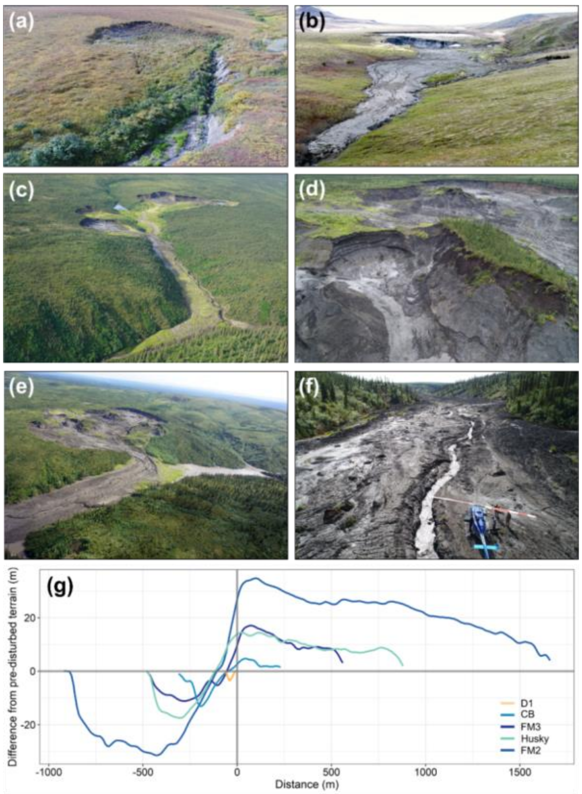
(a)
(b)
(c)
(d)
(e)
(f)
(g)
Difference from pre-disturbed terrain (m)
20
0
-20
-1000
-500
0
500
1000
1500
Distance (m)
D1
CB
FM3
Husky
FM2

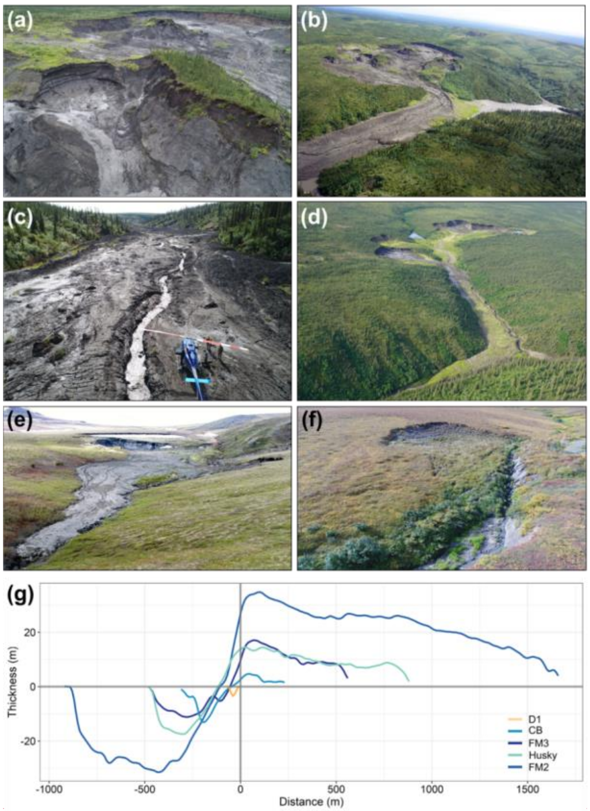
(a)
(b)
(c)
(d)
(e)
(f)
(g)
Thickness (m)
Distance (m)
D1
CB
FM3
Husky
FM2

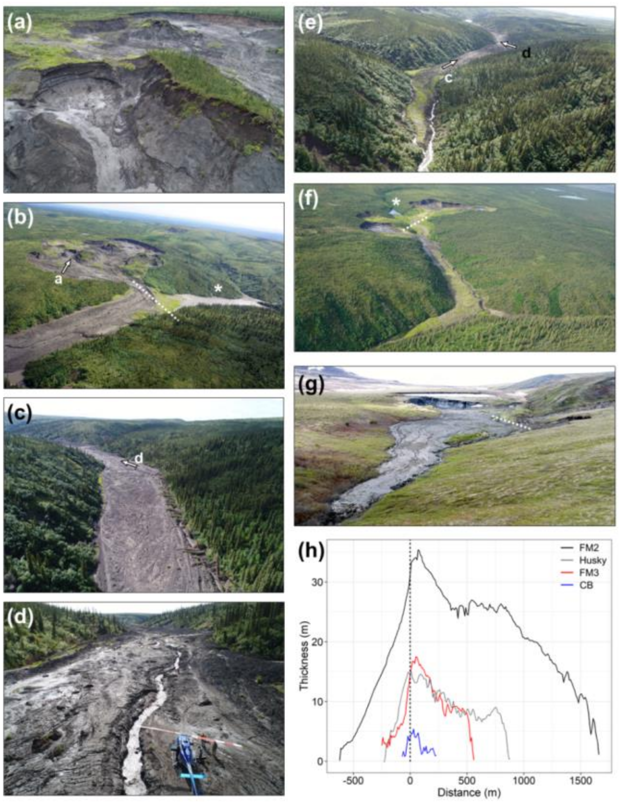

Figure 2. ~~Plate showing~~Examples of retrogressive thaw-slumps and debris tongue deposits (a-f), and elevation normalized scar-zone and debris~~-~~-tongue profiles for a size and age disturbance continuum (g), Peel Plateau, Northwest Territories, Canada. (a) A small, shallow slope-side thaw slump (D1) with vegetated lower slope and active headwall; ~~(a-e) FM2 mega-slump and debris tongue. (a) FM2 headwall retreat showing banded relict massive ice and relatively thaw-stable organic deposit and erosion of glaciofluvial deposit in upper right (background);~~ (b) Oblique photograph of CB in June 2019 showing debris tongue in foreground, secondary slumps on right side of valley, large polycyclic (secondary) headwall in the central scar zone, and small upper (primary) headwall in the background; (c) Husky slump scar and debris tongue, secondary slumps on left, a small debris-dam lake, and slump-drained lake and residual pond to right of upper slump; and (d-f) FM2 mega slump and debris tongue. (d) FM2 headwall showing banded relict massive ice and relatively thaw-stable organic deposits and eroded glaciofluvial deposits in upper right (background); (~~b~~e) FM2 scar area and chute ~~(dotted white line)~~ where sediment enters the valley to form the debris tongue and a~~the~~ debris-dam lake, and ~~(*)~~; (f~~c-e~~) ~~show FM2 debris tongue from several vantage points indicating the magnitude of the~~the debris tongue surface~~colluvial deposit~~ and the stream channel which has started to incise

the deposit.~~, initial stages of stream incision (d), and side valley erosion (c, e); (f) Husky slump scar and debris tongue, secondary slumps on left, debris-dam lake (*) and slump-drained lake and residual pond to right of upper slump; (g) Oblique photograph of CB in June 2019 showing debris tongue in foreground, secondary slumps on right side of valley, large polycyclic (secondary) headwall in the central scar zone, and small upper (primary) headwall with snow patch in background.~~ (~~h~~g) Elevation normalized scar (- values) and debris~~-~~ tongue (+ values) topographic ~~-~~profiles for slumps and debris tongue deposits.~~tudy slumps~~ Profiles are differenced from the pre-disturbed terrain surface. Slope transects are from the slump headwall to the intersection with the stream channel, and downstream transects extend to the end of the debris tongue. Slumps and transects are shown in Figure S1.~~;~~

~~White dashed lines on (b), (f) and (g) indicate 0 m distance on graph (h) where the debris flow enters the downstream channel. Letters and arrows on photographs are reference points indicating location and view of associated photographs.~~

In 2018, the area of slump FM2 was an order of magnitude larger than the other disturbances~~,~~ and ~~has~~ had been a site of recurrent erosion for over half of a century (Lacelle et al., 2015). About 30% of the scar cavity volume (6.0 x 10^6 m^3) has been accounted for in the valley-fill (Table 1; Figs. 2 d-g), consistent with excess ice content estimates of 50 to 70%. Increasing thaw-driven sediment flows, coincide~~d~~nt with the regional ~~acceleration of slump activity~~increase in the frequency and magnitude of thaw slumps in the late 1990s (Kokelj et al., 2015), enlarged~~ing~~ the debris tongue to about 2 km length and 35 m thickness by 2018 (Figs. 2 ~~a~~d-~~g~~f, S1) (van der Sluijs et al., 2018). By filling the trunk valley, these very large deposits flatten the upstream energy profile~~,~~ and create~~ing~~ depositional environments such as the debris-dam lake at FM2 (Fig. 2~~b~~e), which has infilled with sediment~~,~~ supplied from erosion of the FM3 debris tongue situated about 1 km upstream. Fluvial incision of the FM2 debris tongue (Fig. 2~~d~~f) and ~~pinning~~ diversion of the stream channel by the accumulation of colluvial deposits ~~to the valley wall (Fig. 2c) is~~are causing high rates of valley-side erosion. The~~However, the~~ persistence of these ~~massive~~ thick deposits demonstrates that ~~thaw-driven~~ sediment supply exceeds transport capacity of headwater streams by several orders of magnitude.

3.2 The thaw-driven evolution of slope-to-stream connectivity

The abrupt transition of shallow~~mall~~ valley-side thaw ~~-~~slumps into larger, ~~larger,~~ more dynamic failures ~~connected to downstream environments~~that exhibit downstream connectivity is transforming the geomorphology of ice-rich glaciated ~~landscapes~~environments. These dynamics were captured through LiDAR and multi-year UAV observations from Peel Plateau (Fig. 3). Thaw slump CB was initiated by stream erosion around 2002-2004, and gradually back-wasted up an 8 to 12° slope to form a 25,900 m^2 disturbance by 2011, comprised of a shallow scar zone (mean depth = 2.2 m, SD = 2.1 m) with an upper zone of mud slurry and a lower, vegetated accumulation zone (Fig. 3a). The headwall, up to 7.0 m high, exposed the active layer underlain by the early Holocene paleoactive layer and Pleistocene age icy permafrost at depth (Lacelle et al., 2019). In 2015 the scar area had increased to 33,370 m^2 (+29%), but maximum headwall height (5.8 m) and mean concavity depth (1.9 m; SD = 1.9 m) decreased as thawed materials accumulated in the scar zone (Figs. 3b~~, d,~~ e). Over the first ~~a~~ decade of slump growth ~~yielded~~ material redistribution was constrained largely to the slope system, and top-down thaw of ice-rich permafrost within areas of the lower scar zone is suggested by continued subsidence (Fig. 3b). A~~However, a~~

major episode of mass-wasting initiated in summer 2017 evacuated the materials accumulated within the slump scar zone to form a 2.2 x 10^4 m^3 debris tongue comprised of colluvium transported up to 200 m down valley, and a ~12.5-~~–~~m high headwall in the central scar zone concavity. This large, lower headwall observed in fall 2018 exposed about ~~1~~a metre of colluvium overlying icy sediments that extended to a depth of at least 14 m below the pre-disturbance surface (Figs. 2b~~g~~, 3c-e). Gradual retreat of the upper headwall from 2015 to 2018 increased the scar footprint ~~by only~~by less than ~~–~~10~~2~~%, but evacuation of colluvium in 2017-2018 more than doubled the mean depth and total volume of the scar cavity (Fig. 3). Thaw-driven, rainfall-enhanced re-mobilization of scar-zone colluvium coupled the slope and stream valley by transporting~~placing~~ large volumes of erodible substrate into the channel. Evacuation of materials from the scar zone exposed a large secondary headwall strengthening feedbacks that drive slump proliferation (Kokelj et al., 2015).

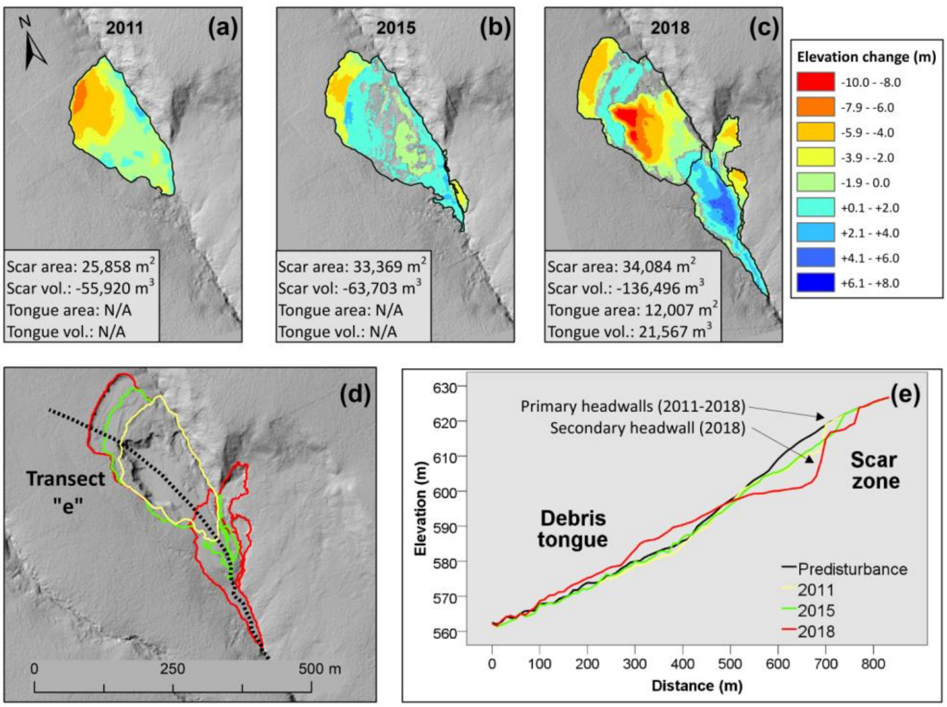
2011
(a)
N
Scar area: 25,858 m2
Scar vol.: -55,920 m3
Tongue area: N/A
Tongue vol.: N/A
2015
(b)
Scar area: 33,369 m2
Scar vol: -63,703 m3
Tongue area: N/A
Tongue vol.: N/A
2018
(c)
Scar area: 34,084 m2
Scar vol.: -136,496 m3
Tongue area: 12,007 m2
Tongue vol.: 21,567 m3
Elevation change (m)
-10.0 - -8.0
-7.9 - -6.0
-5.9 - -4.0
-3.9 - -2.0
-1.9 - 0.0
+0.1 - +2.0
+2.1 - +4.0
+4.1 - +6.0
+6.1 - +8.0
(d)
Transect "e"
0
250
500 m
(e)
Primary headwalls (2011-2018)
Secondary headwall (2018)
Scar zone
Debris tongue
Predisturbance
2011
2015
2018
Elevation (m)
Distance (m)

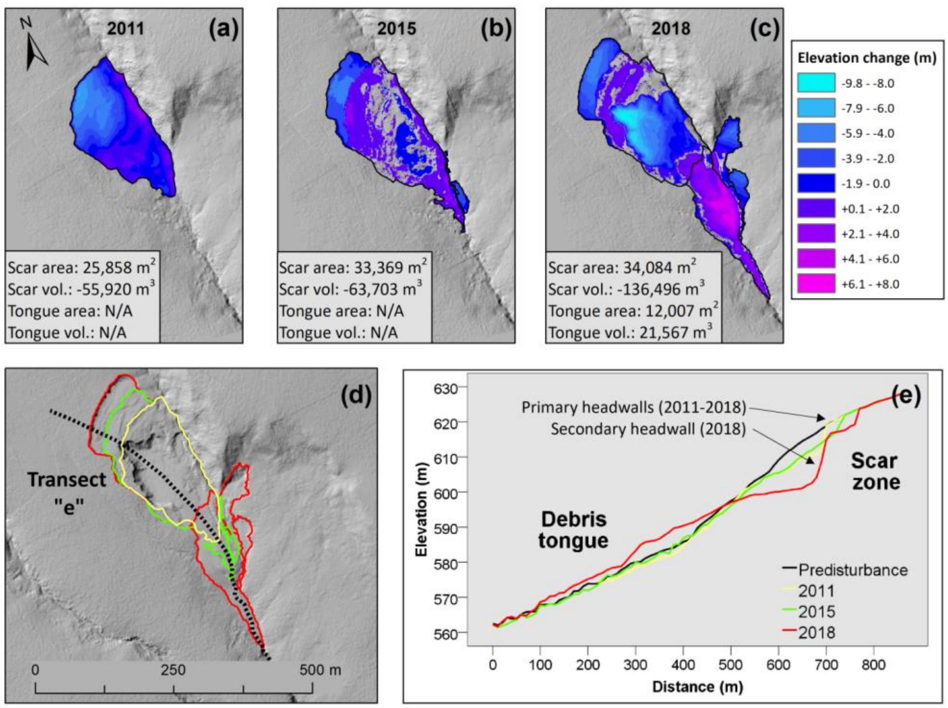

Figure 3. Thaw slump growth (slump CB), material displacement and evolution of downstream connectivity 2011 to 2018, Peel Plateau, Northwest Territories Canada. (a) 2011 difference from the reconstructed pre-disturbance terrain surface; (b) 2015 terrain differenced from the 2011 terrain; (c) 2018 terrain differenced from the 2015 terrain, showing polycyclic behaviour including thaw-driven evacuation of scar materials, and development of a prominent lower "secondary" headwall and scar concavity. Slump and debris tongue area and volumes are calculated~~estimated~~ relative to ~~an estimated~~estimated pre-disturbance surface. (d) The evolution of thaw slump footprint from 2011 to 2018 and the topographic transect in (e) showing ~~cross-sections~~elevation profiles through the slump and along the valley for pre-disturbed terrain, 2011, 2015 and 2018. Hill-shade in (d) is the 2018 UAV survey integrated with the surrounding 2011 regional LiDAR data.

3.3 Quantifying slump enlargement and downstream connectivity across the subarctic to ~~-~~low Arctic transition

Thaw-slump ~~size indices~~area, volume, and maximum concavity depth derived from the 2011 LiDAR study area (Sect. 2.3, Table S1) were compiled to investigate relationships between geomorphology, and downstream connectivity, for the fluvially-incised Peel Plateau and lake-rich Tuktoyaktuk Coastlands and Anderson Plain (Fig. 1). Within the two LiDAR corridors, the digitized scar areas ranged from 242 to 253,900 m^2 with a median of 3,323 m^2. Volume displacement ranged from 130 m^3 to 3,653,400 m^3 with a median of 3,859 m^3, and the maximum difference between estimated pre-disturbance surface and disturbed scar surface (referred to as maximum concavity depth) ranged from -1.5 m to -28.0 m with a median of -3.4 m for the sampled population (Table S3~~2~~). The accumulation of thawed colluvium on the lower slope of smaller slope-side disturbances can produce lobes that manifest as positive relief features (Figs. 3a, b). The larger disturbances were characterized by entirely negative relief relative to the pre-disturbance terrain. The slump size ~~indices~~ metrics are distributed across 3-4 orders of magnitude in scale, indicating the geomorphic significance of the large~~rst~~ features. ~~Paired t-tests~~T-tests on log-transformed data indicated that the mean of all slump size metrics~~indices~~ (area, volume, and maximum concavity depth) for the higher relief, fluvially-incised Peel Plateau were significantly greater ($P<0.02$) than in the rolling, lake-rich terrain of the Anderson Plain and Tuktoyaktuk Coastlands.

Thaw slump populations were grouped by their connectivity with the downstream environment. One-way ANOVA indicated significant differences in the means amongst downstream connectivity groups for slump area ($F_{2, 68}$=32.6 $P<0.001$), concavity volume ($F_{2,68}$=40.9; $P<0.001$), and maximum concavity depth ($F_{2, 68}$= 35.2; $P<0.001$) (Fig. S~~1~~2). Tukey's HSD post-hoc test indicated significant differences amongst all connectivity groups with disturbance area ($P<0.02$), volume ($P<0.005$), and maximum concavity depth ($P<0.017$), ~~increasing with the~~demonstrating that ~~strengthening of~~ downstream connectivity increases with slump size. This pattern supports Sect.~~subsections~~ 3.1 and 3.2, and indicate~~ing~~ that disturbance enlargement is linked to the coupling of slopes and downstream systems.

To further explore the slope-scale geomorphic implications of slump enlargement, we examined the relationships between slump scar area and volume, and scar area and maximum concavity depth. A linear model fit through the logarithmically-transformed disturbance area and volume data (Fig. 4a) reveals a power-law relationship (R^2 = 0.90; F=641.9; N=71; $P<0.0001$):

$$(\log \text{Volume}) = -1.44 + 1.42(\log \text{Area}) \qquad \text{(Eq. 1)}$$

The model coefficients are comparable with those describing area-volume relationships of landslide populations for ~~a number of~~ studies from temperate environments across a range of failure mechanisms, material properties and geological settings (Klar et al., 2011). Figure 4b shows the power-law relationship (R^2 = 0.63; F=116.2; N=71; $P<0.0001$) between scar area and maximum concavity depth described by:

$$(\log \text{Concavity Depth}) = -0.76 + 0.36 (\log \text{Area}) \qquad \text{(Eq. 2)}$$

where the depth of permafrost thawed generally increases as thaw slumps enlarge. Residual ~~S~~scatter in both of these relationships reflects inherent differences in landscape, soil properties, geomorphic setting, and the stage of slump development (Figs. 2, 3). However, the relationships indicate that slump area can be used to estimate the volume and thicknesses of permafrost thawed, improving our ability to quantify the role of thermokarst mass wasting in landscape evolution. Further investigations are required to determine whether these relationships will vary with landscape, material properties, and failure mechanisms.

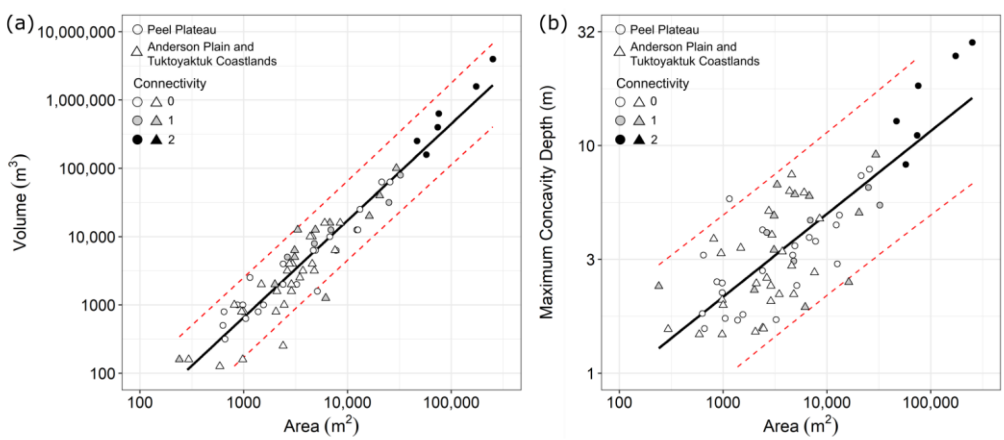

Figure 4. Relationships between: (a) slump scar area and volume (R^2 = 0.90; F=641.9; N=71; P<0.0001), and (b) slump scar area and maximum depth of concavity (R^2 = 0.63; F=116.2; N=71; P<0.0001) for disturbances in the fluvially-incised Peel Plateau, and lake dominated Anderson Plain and ~~/~~Tuktoyaktuk Coastlands. Connectivity between slope and downstream environment is categorized by: “0”~~)~~ no connectivity; “1~~)~~” physical connection between bare scar and downstream environment; and “2~~)~~” evidence of downstream deposition of materials into valley, stream channel or lake. Red ~~dotted~~ dashed lines show 95% confidence limit. Regression diagnostics indicate that residuals are normally distributed, and there are no unduly influential points.

3.4 Analysis of catchment-scale ~~slope thermokarst~~slope thermokarst effects, Willow River

Thaw-driven mass wasting and slope denudation for 1986-2018 were quantified for the 80~~0~~6 km^2 Willow River catchment (Fig. 1). The fluvially-incised stream network drains ice-rich glacial tills and unglaciated scree slopes of the Richardson Mountains into the Mackenzie Delta. Retrogressive thaw slumps are the dominant mode of slope failure; however, extensive field observations confirm that shallow landslides and few large translational failures also occur (Fig~~s~~. ~~6,~~ S~~2~~3) (Lacelle et al., 2010). Bare or sparsely vegetated thaw-slump scar and debris tongues mapped using Landsat imagery (Rudy and Kokelj, 2020) indicated a fourfold increase in the number of active thaw slumps from 1986 to 2002, and another 2.5-fold increase by 2018 (Fig. 5a). These results contrast with earlier assessment by Lacelle et al., (2010) in part due to a ~~significantly~~ larger catchment area in this study, different time scales, and nature of imagery utilized. We employed the empirical models ~~developed in Sect~~(Fig. 4)~~ion 3.3,~~ to convert digitized slump scar areas to estimates of slump volume and ~~depth of~~ maximum ~~thaw~~concavity depth for the three time periods. Cumulative disturbance area and volume showed 34- and 80~~-~~-fold increases, respectively, over the intervals of record (Figs. 5b, c). The median area of ~~the~~ active thaw slump populations for 1986, 2002 and 2018 was 4,510 m^2, 5,680 m^2 and 8,290 m^2, respectively (Fig. 5d, Table S~~3~~4). Comparison with mean values for the same time periods of 5,000 m^2, 9,770 m^2 and 17,910 m^2 (Table S4~~3~~) highlights the increasingly skewed nature of the population distributions as disturbances enlarge (Kokelj et al., 2015). Approximated mean slump volumes and maximum concavity depths of active thaw slumps increased over time and were, respectively,~~ in 1986 were~~ 6,900 m^3~~,~~ and 3.6 m in 1986, ~~increasing to~~ 19,690 m^3 ~~,~~and 4.1 m in 2002, and~~ to~~ 59,030 m^3~~,~~ and 5.1 m by 2018 (Table S~~3~~4). The~~ estimated~~ volumes of the largest disturbances have increased by two orders of magnitude, and there has been at least a three-fold increase in ~~the approximated~~ maximum concavity depth (Fig. 5), although the models appear to provide conservative ~~high-~~high-end estimates of both parameters (Fig. 4). Kruskall-Wallis rank sum tests indicated significant differences in slump size indices amongst the different time periods ($\chi^2(2) = 22.825$; $P<0.0001$). Dunn's post-hoc testing showed no significant increases in disturbance area, volume, or maximum concavity depth from 1986 to 2002, however, increases in the population medians were significant for all size-related indices from the first two time periods to 2018 (Figs. 5d-f; Table S~~4~~5), suggesting a period of slump initiation followed by accelerated enlargement from about 2002~~-~~ to 2018. During the 2002-2018 period, development of numerous debris-tongue deposits indicates major strengthening of~~ connectivity between~~ slope to~~s and~~ stream connectivity~~s~~ (Fig. 5a). The catchment-wide cumulative slump volume estimates of 0.15 x 10^6 m^3 in 1986, 1.43 x 10^6 m^3 in 2002 and 11.70 x 10^6 m^3 in 2018 reveal a non-linear increase in thaw-driven geomorphic activity across two orders of magnitude over three decades (Fig. 5c).

A significant proportion of volume loss from slopes can be attributed to ground ice melt and water loss, and a large portion of the mobilized slope materials are placed into transient storage in valley bottoms (Fig. 2). To translate the significant increases in thaw-driven geomorphic activity into values that can be compared with surface denudation rates of ~~from~~catchments in other regions, we ~~N~~normalized the combined subsidence and erosional volume losses~~ing~~ by catchment area and differenced~~ing~~ with the preceding time interval. These calculations indicate that for Willow River watershed,~~,~~ the thaw slump component of surface lowering or volumetric loss amounts to 0.1 mm yr^{-1} or mobilization rates of 100 m^3 km^{-2} yr^{-1} for 1986-2002 and 0.~~8~~79 mm yr^{-1} ~~-~~or 794~~800~~ m^3 km^{-2} yr^{-1} for 2002-2018. In a relatively quiescent landscape that is frozen for almost two-thirds of the year, this represents a dramatic change in the geomorphology and ~~geomorphology and~~ sediment delivery regime ~~regime~~ from thawing slopes to the stream systems.

~~The major intensification of thaw-driven mass wasting in the Willow River catchment (Fig. 5) predominantly occurs on the uppermost slopes in the drainage networks, mainly affecting first and second-order streams (Fig. 6). The exposure of several kilometres of slump headwall confirms that the low-order stream networks are incising ice-rich glaciated terrain and that the majority of materials mobilized by the largest disturbances comprise Pleistocene sediments and relict ground ice (Fig. 6; Video S2). Steeply-incised valley sides of fourth and fifth-order channel segments which occupy the broader valley of Willow River main stem are also affected by a number of large, deep-seated translational failure complexes (Figs. 6, S2) that exhibit bedrock control, as well as thaw-driven flows. The incised valleys are susceptible to shallow landslides, and although they transfer comparatively modest amounts of sediment to the stream network, they contribute to thaw slump initiation by exposing ground ice on steep slopes. Our mapping of the Willow River catchment indicates that 116 km out of 861 km of stream segment length was directly affected by slope thermokarst, with downstream accumulation increasing the length of the affected network by 246 km, to 42% of the entire stream network. The downstream translation of thaw-driven slope sediment mobilization (Figs. 5, 6) through the Willow River fluvial network is indicated by the rerouting of the outflow channel to the Mackenzie Delta in 2007-2008, leading to the rapid infilling of a 3.4 km^2 lake over the span of a decade (Fig. 6c; Video S3).~~

Formatted: Not Highlight

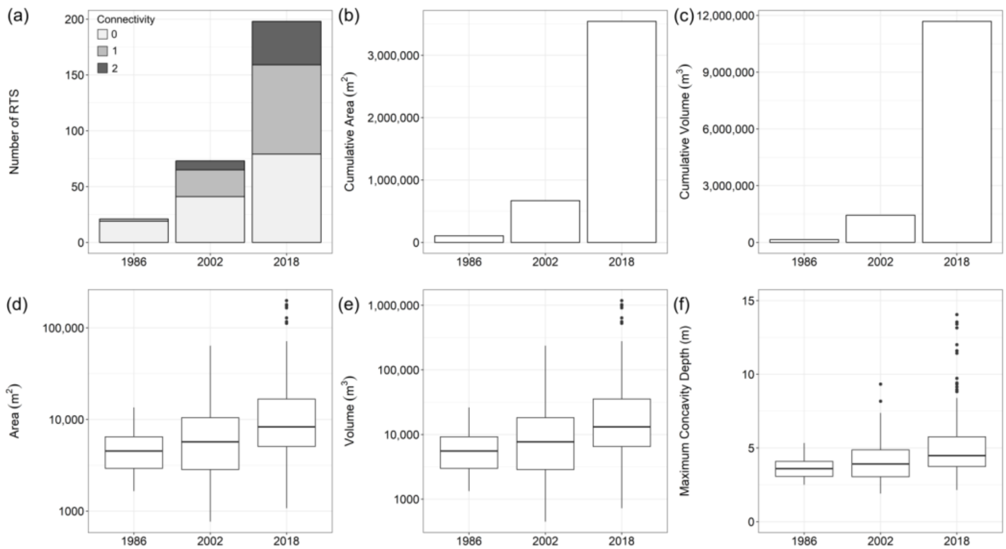

(a)
Connectivity
0
1
2
Number of RTS
0
50
100
150
200
1986
2002
2018
(b)
Cumulative Area (m2)
0
1,000,000
2,000,000
3,000,000
(c)
Cumulative Volume (m3)
0
3,000,000
6,000,000
9,000,000
12,000,000
(d)
Area (m2)
1000
10,000
100,000
(e)
Volume (m3)
1000
10,000
100,000
1,000,000
(f)
Maximum Concavity Depth (m)
0
5
10
15

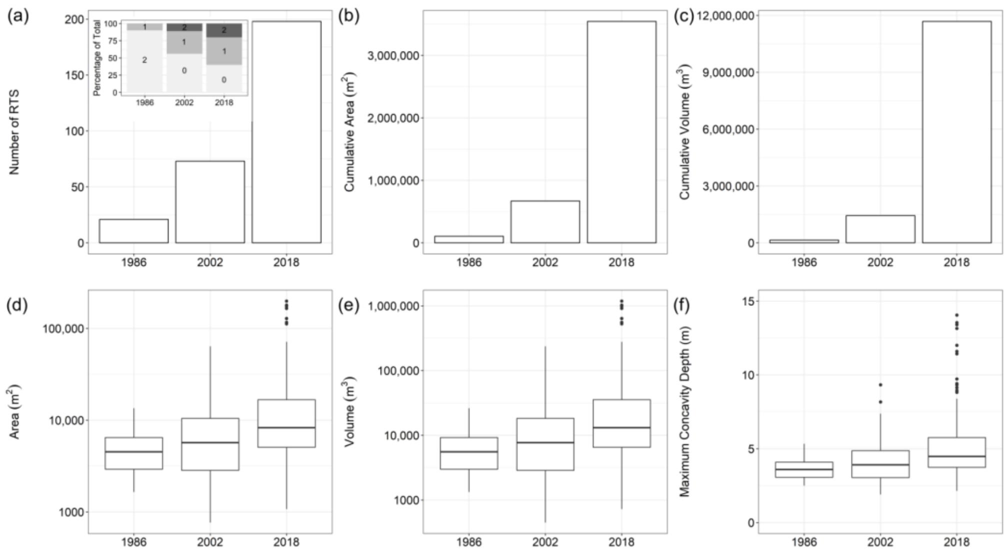

Figure 5. Thaw-driven geomorphic disturbances in the Willow River catchment for 1986, 2002 and 2018. Bar graphs show: (a) Slump counts and connectivity between the slope and downstream environments categorized as “0” no connectivity, “1” physical connection between bare scar area and downstream environment, and “2” evidence of downstream deposition of materials into valley, stream channel or lake~~with inset showing proportion of retrogressive thaw slumps (RTS) with downstream connectivity~~;~~,~~ (b) cumulative slump area;~~,~~ and (c) estimated cumulative slump volume. Box and whisker plots showing medians, 25% and 75% quantiles, minimum and maximum values, and outliers for:~~;~~ (d) thaw slump area;~~,~~ (e) approximated volumes;~~,~~ and (f) maximum concavity ~~thicknesses~~depths. Note logarithmic scale on (d) and (e). ~~On Plot (a) inset, the connectivity between the slope and downstream environments is categorized by 0) no connectivity, 1) physical connection between bare scar area and downstream environment, and 2) evidence of downstream deposition of materials into valley, stream channel or lake.~~ Thaw slump volume and maximum concavity depth~~thicknes~~s estimated using relationships ~~shown~~ described in Sect. 3.3 and Figure 4. The spatial dataset is available in Rudy and Kokelj, 2020~~a~~.

The major intensification of thaw-driven mass wasting in the Willow River catchment predominantly occurs on the uppermost slopes in the drainage networks, mainly affecting first, and second-order streams (Fig. 6). The exposure of several kilometres of slump headwall confirms that the low-order stream networks are incising ice-rich glaciated terrain~~,~~ and that the majority of materials mobilized by the largest disturbances comprise Pleistocene sediments and relict ground ice (Fig. 6; Video S2). Steeply-incised valley sides of fourth~~,~~ and fifth-order channel segments which occupy the broader valley of Willow River main stem are also affected by a number of large, deep-seated translational failure complexes (Figs. 6, S3) that can exhibit bedrock control, as well as thaw-driven flows. The incised valleys are susceptible to shallow landslides, and although they transfer comparatively modest amounts of sediment to the stream network, they contribute to thaw slump initiation by exposing ground ice on the upper slopes. Our mapping of the Willow River catchment indicates that 116 km out of 861 km of stream segment length were directly affected by thermokarst mass-wasting features, with downstream accumulation increasing the length of the affected network by 246 km~~,~~ to 42% of the entire stream network. The downstream translation of sediments mobilized by thaw-driven mass wasting (Figs. 5, 6) through the Willow River fluvial network is indicated by the rerouting of the outflow channel to the Mackenzie Delta in 2007-2008, leading to the rapid infilling of a 3.4 km^2 lake over the span of a decade (Figs. 6c1-2; Video S3).

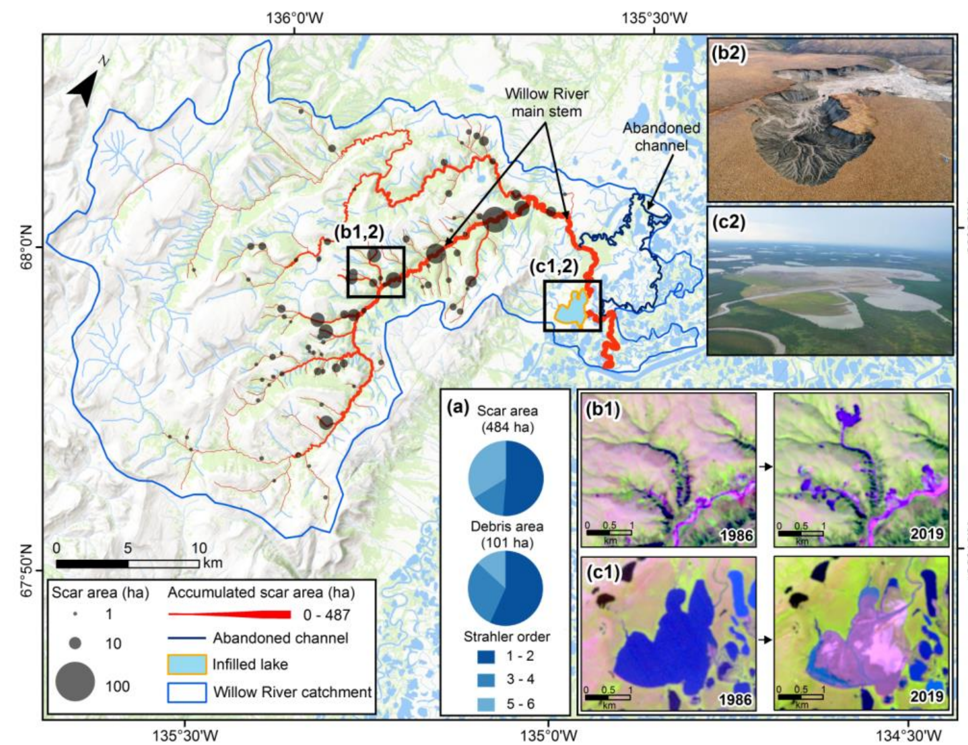
136°0'W
135°30'W
Willow River main stem
Abandoned channel
(b2)
(c2)
(b1,2)
(c1,2)
68°0'N
68°20'N
67°50'N
68°10'N
0 5 10 km
Scar area (ha)
1
10
100
Accumulated scar area (ha)
0 - 487
Abandoned channel
Infilled lake
Willow River catchment
(a)
Scar area (484 ha)
Debris area (101 ha)
Strahler order
1 - 2
3 - 4
5 - 6
(b1)
1986
2019
(c1)
1986
2019
135°30'W
135°0'W
134°30'W

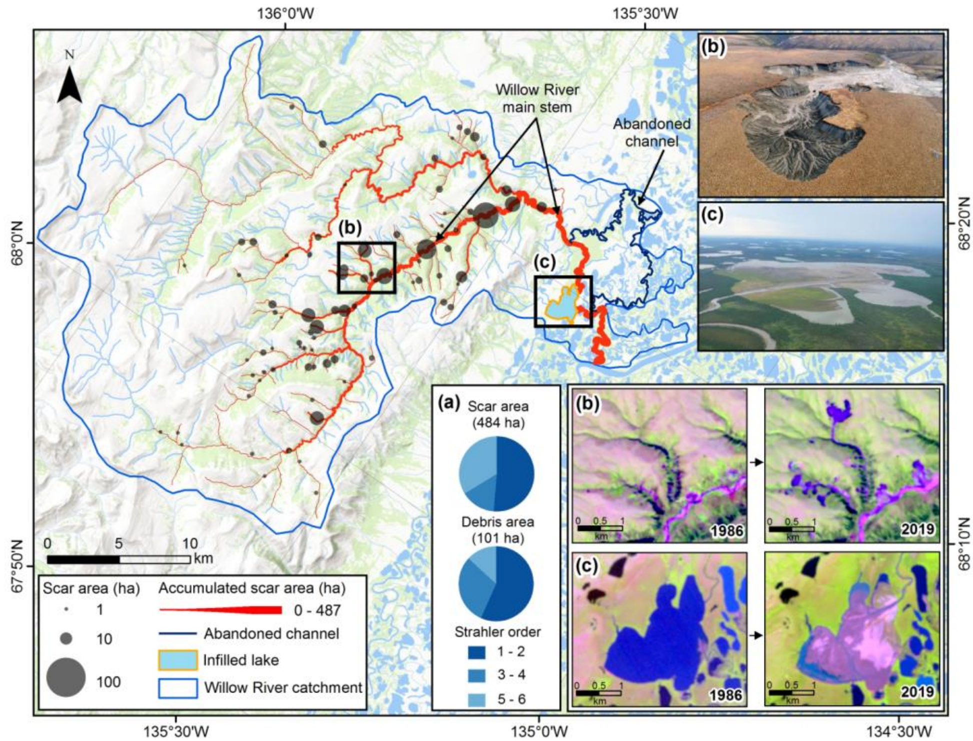

Figure 6. Main map shows ~~T~~thaw-driven landslide impacts to the fluvial network of the Willow River, Mackenzie Delta area. Red lines along the drainage network highlight impacted stream segments, weighted by cumulative ~~slope thermokarst~~landslide scar area (ha), and the downstream accumulation of impacts through the fluvial system. The ~~black~~ grey proportional circles indicate the total landslide scar area >1ha per affected stream segment, including thaw slump, and shallow and deep translational slides. The abandoned channel is shown in dark blue. Boxes on map labelled (b1, 2) and (c1, 2) indicate inset imagery and photographs. (a) The ~~area~~ area-weighted distribution of thaw-driven landslide impacts by Strahler order within the Willow River fluvial network. (b1) Landsat images (1986-07-07) and (2019-07-27) indicating increases in thaw-driven landslide erosion ~~developed~~ since the late 1990s, and (b2) corresponding oblique aerial photograph~~s~~ of the largest thaw slump within the Landsat plate. (c1) Landsat images for the same dates show~~of rapid lake infilling~~the lake before and after infilling and ~~and~~ delta development where Willow River rerouted in 2007-2008 into Willow Lake ~~(outlined in Orange), Mackenzie Delta~~, and (c2) oblique photograph of the alluvial deposit~~showing the new alluvial deposit~~. Landsat images are false colour composites of multispectral bands, with R = shortwave infrared, G = near infrared, and B = green. ~~The abandoned channel is shown in dark blue.~~ Base map is from ESRI ArcGIS Online.

3.5 Catchment-scale patterns of ~~thaw slump~~thaw-driven mass wasting effects and sediment flux across catchment scales

The patterns of~~ slope~~ slope thermokarst distribution and intensification were assessed across catchment scales for a 3,520 km^2 area on Peel Plateau and ~~contrasted with a~~a contrasting 1,220 km^2 area on southeastern Banks Island (Fig. 1). The distribution of slope disturbance determined from SPOT 4/5 200~~4~~5-2010~~05~~ and 201~~8~~6-2017 Sentinel-2 imagery on Peel Plateau shows increasing frequency across all size classes (Fig. 7a). This pattern reflects initiation of new disturbances ~~including some smaller slides~~, as well as~~ perpetuation and~~ thaw-driven enlargement of existing slope failures~~features~~. On southeastern Banks Island, overall slope disturbance density was greater, but the relative increase ~~in disturbance incidences~~ over the past decade was lower than for Peel Plateau. A distinct shift towards larger ~~features~~ thaw slumps on Banks Island suggests disturbance growth and coalescence (Fig. 7b). Figure 7c provides a cumulative summary of the points at which the river network is being impacted by ~~major~~ thaw-driven mass wasting~~ activity~~. Evidently, ~~major~~ thaw slumps and slides~~disturbances~~ tend to impact the channel at 1-100 km^2 catchment scales, consistent with patterns observed for Willow River (Fig. 6a). The temporal shift from 2005-2010 to 2016-2017 towards a relative increase in direct effects to larger channels in the Peel Plateau region reflects the greater watershed sizes, and thus more available downstream terrain for new disturbance ~~proliferation~~impacts (Fig. 7c). Some of the main Peel River tributaries are becoming increasingly ~~being~~ affected by large slope thermokarst failures and shallow slides similar to those observed in the Willow River catchment (Figs. 6, S3). On Banks Island, the smaller fluvial networks were already highly impacted by thaw slumping in 2005 (Segal et al., 2016a, Lewkowicz and Way, 2019), leaving less available terrain for expansion of direct network impacts, as indicated by ~~the slightly~~smaller~~ more subdued~~ increases in slump incidence (Fig. 7b), and a static pattern in distribution of catchment disturbances between the two time periods (Fig~~s~~. 7~~b, ~~c). Figure 7d reinforces that the geomorphic and geochemical impacts to headwater streams tend to be more intense than direct impacts to larger systems~~,~~ because the size of the disturbance relative to the watershed area will be far greater. Further downstream, the overall impacts from individual disturbances and cumulative effects will be proportionately less, given the much larger upstream catchment area ~~(i.e. trunk channel discharge)~~ and greater stream transport capacity~~,~~ relative to sedimentary or geochemical yields from the disturbance.

There is a notable dearth of river sediment monitoring over the vast, thermokarst sensitive regions of northwestern Canada. A compilation of available grab samples of stream sediment concentrations coinciding with discharge measurements ~~(Shakil et al., 2020b)~~ within and adjacent to Peel River basin for catchments from 10^{-1} to 10^4 km^2 indicates a negative trend in specific low-flow fluxes with catchment area (Shakil et al., 2020b)~~, consistent with observations of suspended sediment concentrations in glaciated permafrost terrain reported by Kokelj et al., (2017a).~~. Estimates of low-flow sediment fluxes for small ~~thaw-slump affected~~ catchments affected by thaw-driven mass wasting are up to two orders of magnitude greater than for larger watersheds, and several orders of magnitude greater than for undisturbed and unglaciated catchments (Fig. 7e).

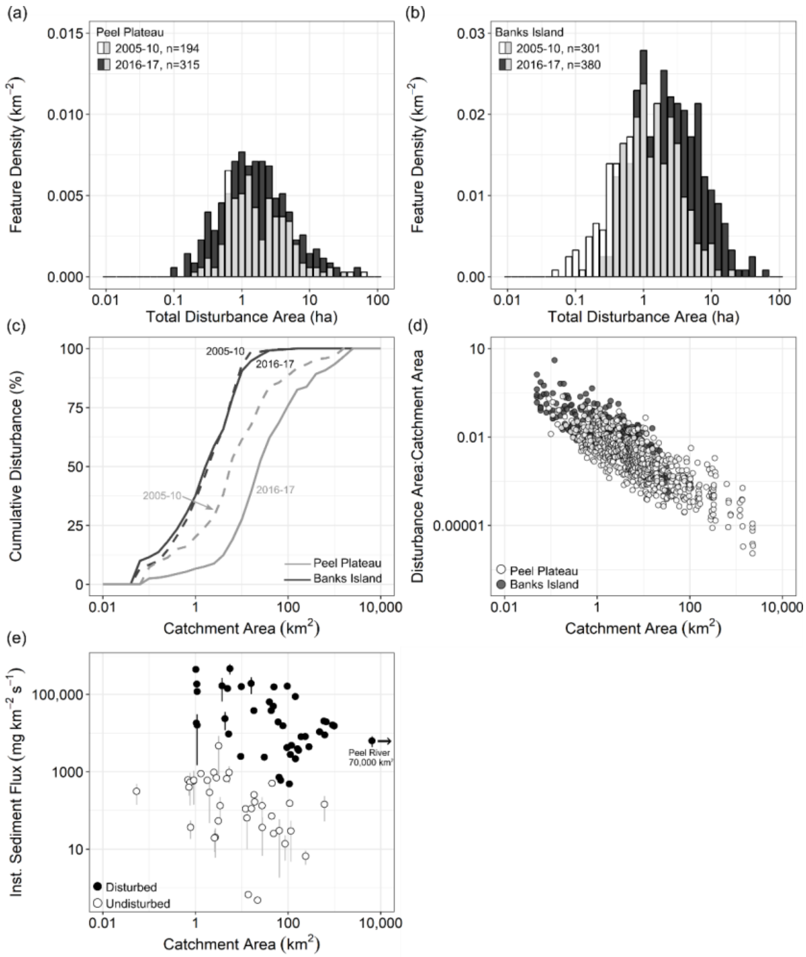

(a)
Peel Plateau
2005-10, n=194
2016-17, n=315
Feature Density (km^{-2})
Total Disturbance Area (ha)
(b)
Banks Island
2005-10, n=301
2016-17, n=380
Feature Density (km^{-2})
Total Disturbance Area (ha)
(c)
Cumulative Disturbance (%)
2005-10
2016-17
Peel Plateau
Banks Island
Catchment Area (km^2)
(d)
Disturbance Area:Catchment Area
Peel Plateau
Banks Island
Catchment Area (km^2)
(e)
Inst. Sediment Flux (mg km^{-2} s^{-1})
Peel River
70,000 km^2
Disturbed
Undisturbed
Catchment Area (km^2)

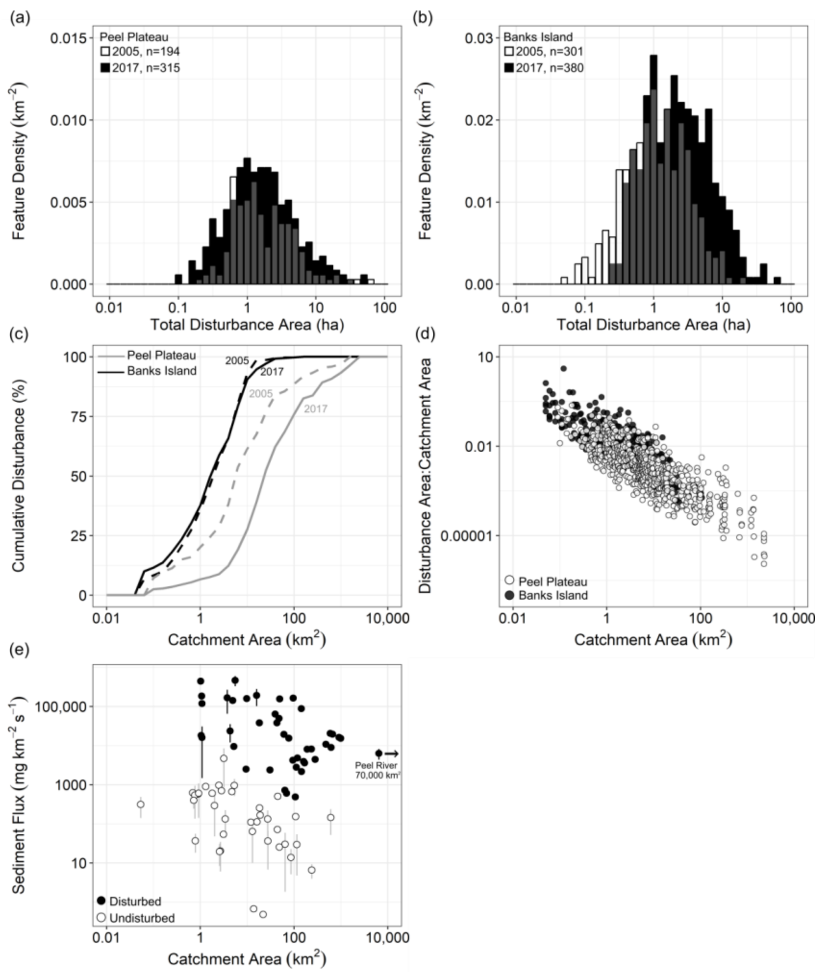

Figure 7. The patterns of thaw slump intensification in fluvial networks for 2005~~4~~-20~~05~~10 and 2016-2017 in Peel Plateau (3,520 km^2) and eastern Banks Island (1,220 km^2) regions. (a, b). Size distribution of thaw slumps for the two time periods where white indicates 2005~~4~~-20~~05~~10, black indicates 2016-2017~~8~~, and ~~grey indicates~~shading shows overlap between 200~~4~~5-2010~~05~~ and 2016-2017~~8~~ distributions; (c) Cumulative count of thaw slumps ~~thaw-slump disturbance count~~ plotted against upstream catchment area; (d) The ratio of disturbance area

to upstream catchment area plotted against upstream catchment area; and (e) July-September instantaneous sediment flux rates for ~~streams and rivers the~~streams of the Peel watershed and adjacent areas.

3.6 ~~Slope thermokarst~~Thaw-driven mass wasting effects propagate through hydrological networks to the ocean

Here we project the potential cascade of slope thermokarst effects through Arctic drainage networks from ~~continuous~~ permafrost terrain of northwestern Canada (Fig. 8). The summary of active ~~slope thermokarst~~permafrost landslides by Strahler stream order for Banks Island (70,794 km^2), Amundsen Gulf (90,288 km^2), Peel River (76,506 km^2), and Keele-~~/~~Redstone (39,957 km^2) watersheds indicates that the greatest abundance and highest density of directly affected ~~thermokarst~~ stream segments was on Banks Island (11.8/1000 km^2) and the lowest was in the Amundsen Gulf (2/1000 km^2). However, major thermokarst hotspots associated with ice-rich moraine, glaciofluvial and glaciolacustine materials occur within all four watersheds where slope disturbance densities are an order of magnitude greater than the watershed average. About 71% of direct ~~slope thermokarst~~thaw-driven mass wasting effects to streams, and over 81% of direct effects to lakes occur within first and ~~second~~ second-order hydrological segments (Fig. 8a), corroborating catchment-scale patterns (Figs. 6, 7), and indicating that thousands of small streams and hundreds of lakes across northwestern Canada are directly affected by slope thermokarst disturbances (Fig. 8b). The ~~major direct~~main impacts~~effects~~ of thaw-driven mass-wasting on hydrological networks are concentrated in well-defined geographical areas, with large regions free of major ~~thaw-driven mass-wasting~~slope thermokarst. For Banks Island and the Peel and Keele-Redstone watersheds, low disturbance densities occur west of the late Wisconsinan ice-limit. ~~Slope thermokarst~~Thaw-driven landslides were ~~was~~ sparse in unglaciated Cordilleran areas and glaciated Precambrian Shield with patchy till veneer. Low disturbance density also characterizes the Taiga Plains of central Mackenzie Valley, however, some valleys incised in~~ing~~ tills and glaciolacustrine deposits are ~~subject~~prone to thaw-related failures, including the Mackenzie River main stem (Figs. 8, S~~3~~4iii).

As a broad summary, ~~slope thermokarst~~thaw-driven mass wasting ~~activity~~ directly affects over 6,750 km of stream segment length, 1,370 lakes and about 900 km of coastline in the ~~continuous permafrost~~Arctic drainage area ~~area~~ of northwestern Canada (Fig. 8). ~~About~~ Approximately 48,800 km of stream network and over 5,600 lakes are susceptible to ~~downstream~~ indirect ~~or "indirect"~~ effects, reflecting 7.2- (streams) and 4.1- (lakes) fold increases over the extents of direct hydrological effects. The much greater extents of downstream effects (Fig. 8a) occur because ~~slope~~ thermokarst mass wasting predominantly impacts low-order streams, often in headwaters of the ~~hydr~~hydrological network. A high density of ~~slope thermokarst~~thaw slumps ~~features~~ ~~connected through~~affecting small streams~~fluvial systems~~ that drain eastern Banks Island and northwestern Victoria Island indicate~~ing~~ major ~~potential to~~ propagation of~~e~~ sedimentary and geochemical effects directly to the coastal zones of the Prince of Wales Strait (Fig~~s. 7c,~~ 8). Northeast of the Mackenzie Basin, several major Arctic river ~~Several Arctic~~ catchments~~drainages northeast of the Mackenzie Basin with~~ have~~-~~ areas of high ~~slope thermokarst~~landslide density with the ~~have the~~ potential to propagate downstream effects.~~-~~ Ice-rich ~~permafrost characterizing a diversity of ice-marginal~~ glacigenic deposits ~~of the Anderson Plain and Tuktoyaktuk Coastlands (Fig. 8ii)~~ of Anderson Plain and Tuktoyaktuk Coastlands surround the Husky Lakes estuary, which is influenced~~integrates the effects of~~ by shoreline slumping, discharge from numerous small slump-affected, lake-dominated catchments, and a few slump-affected northward-flowing rivers, indicating a regional hotspot of accumulated effects (Figs. 8, S4ii~~3~~). Coastal slumping~~erosion~~ along the Yukon North Slope and uplands east of Mackenzie Delta, in conjunction with lake-side slumps, comprise~~disturbances drive~~ the majority of ~~slope thermokarst~~mass-wasting processes there, whereas fluvial transfer from inland impacts~~areas~~ to the coast is ~~relatively~~ limited. High ~~The highest~~ densities of thermokarst~~y of~~ mass wasting affect~~slope thermokarst affects numerous~~ numerous ~~high-energy,~~ fluvial-incised networks draining ice-rich glaciated landscapes of the lower Mackenzie and Peel River basins, so ~~and th~~these two~~ese~~ major rivers~~ systems~~ propagate the greatest magnitude~~s~~ of thaw-driven sedimentary and geochemical effects to the Mackenzie Delta and Beaufort Sea (Fig. 8).

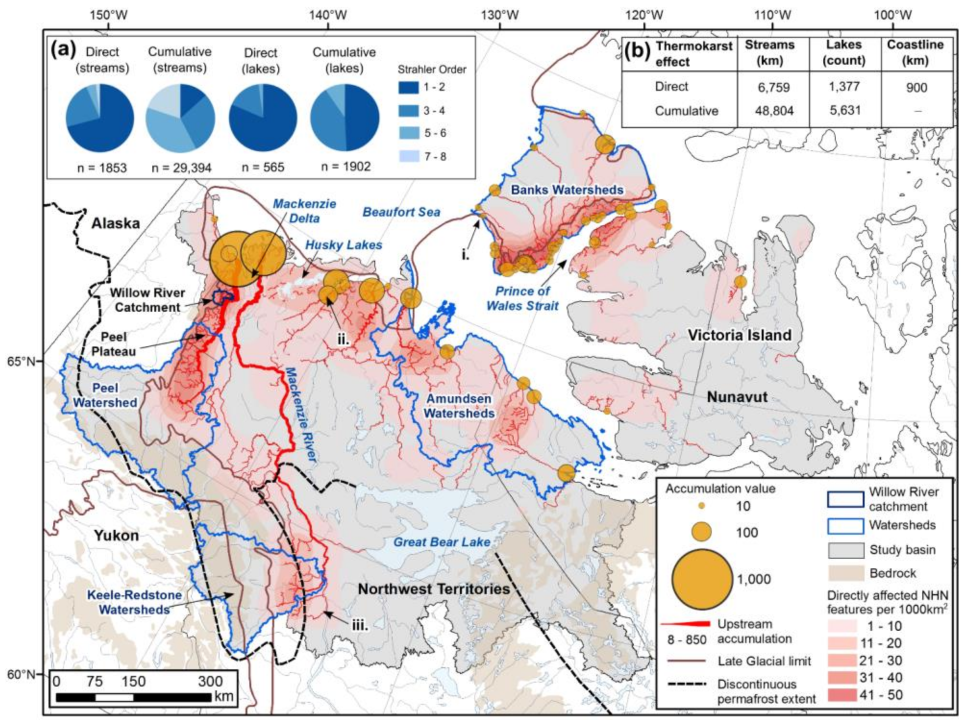

150°W
140°W
130°W
120°W
110°W
100°W
65°N
60°N
(a)
Direct (streams)
Cumulative (streams)
Direct (lakes)
Cumulative (lakes)
Strahler Order
1 - 2
3 - 4
5 - 6
7 - 8
n = 1853
n = 29,394
n = 565
n = 1902
(b)
Thermokarst effect
Streams (km)
Lakes (count)
Coastline (km)
Direct
6,759
1,377
900
Cumulative
48,804
5,631
–
Alaska
Mackenzie Delta
Beaufort Sea
Husky Lakes
Banks Watersheds
i.
Prince of Wales Strait
Willow River Catchment
ii.
Peel Plateau
Victoria Island
Peel Watershed
Mackenzie River
Amundsen Watersheds
Nunavut
Yukon
Great Bear Lake
Northwest Territories
Keele-Redstone Watersheds
iii.
0 75 150 300 km
Accumulation value
10
100
1,000
Upstream accumulation
8 - 850
Late Glacial limit
Discontinuous permafrost extent
Willow River catchment
Watersheds
Study basin
Bedrock
Directly affected NHN features per 1000km²
1 - 10
11 - 20
21 - 30
31 - 40
41 - 50

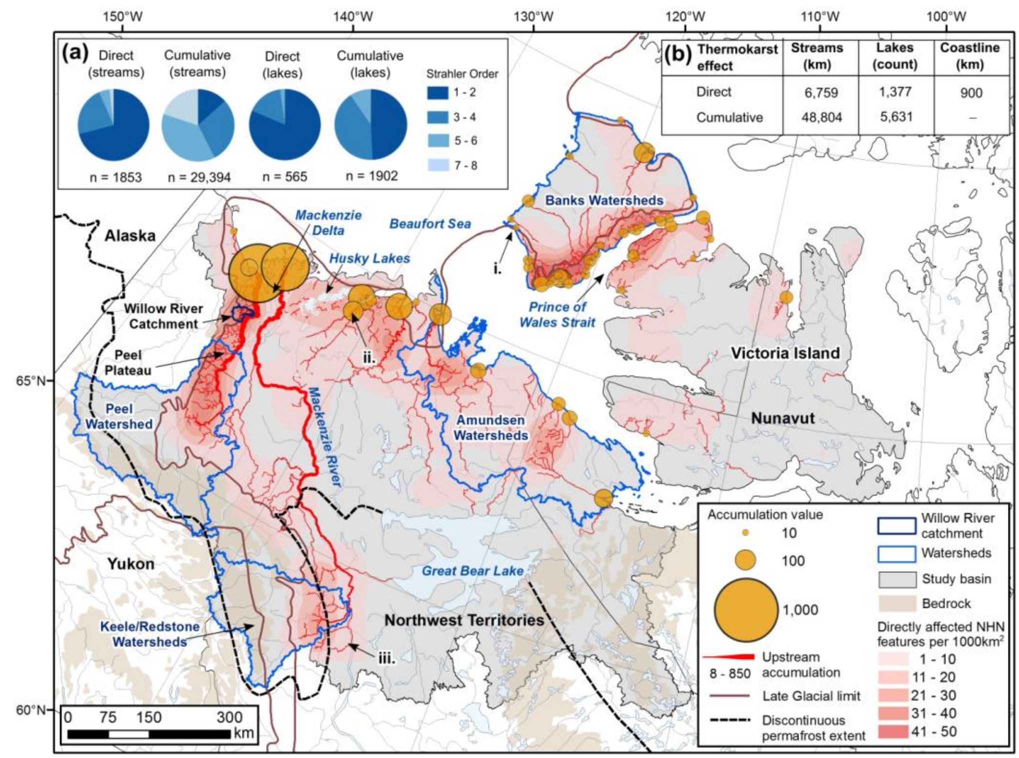
150°W
140°W
130°W
120°W
110°W
100°W
65°N
60°N
(a)
Direct (streams)
Cumulative (streams)
Direct (lakes)
Cumulative (lakes)
Strahler Order
1 - 2
3 - 4
5 - 6
7 - 8
n = 1853
n = 29,394
n = 565
n = 1902
(b)
Thermokarst effect
Streams (km)
Lakes (count)
Coastline (km)
Direct 6,759 1,377 900
Cumulative 48,804 5,631 –
Alaska
Mackenzie Delta
Beaufort Sea
Husky Lakes
Banks Watersheds
i.
Prince of Wales Strait
Willow River Catchment
ii.
Peel Plateau
Victoria Island
Peel Watershed
Mackenzie River
Amundsen Watersheds
Nunavut
Yukon
Great Bear Lake
Keele/Redstone Watersheds
Northwest Territories
iii.
0 75 150 300 km
Accumulation value
10
100
1,000
Upstream accumulation
8 - 850
Late Glacial limit
Discontinuous permafrost extent
Willow River catchment
Watersheds
Study basin
Bedrock
Directly affected NHN features per 1000km²
1 - 10
11 - 20
21 - 30
31 - 40
41 - 50

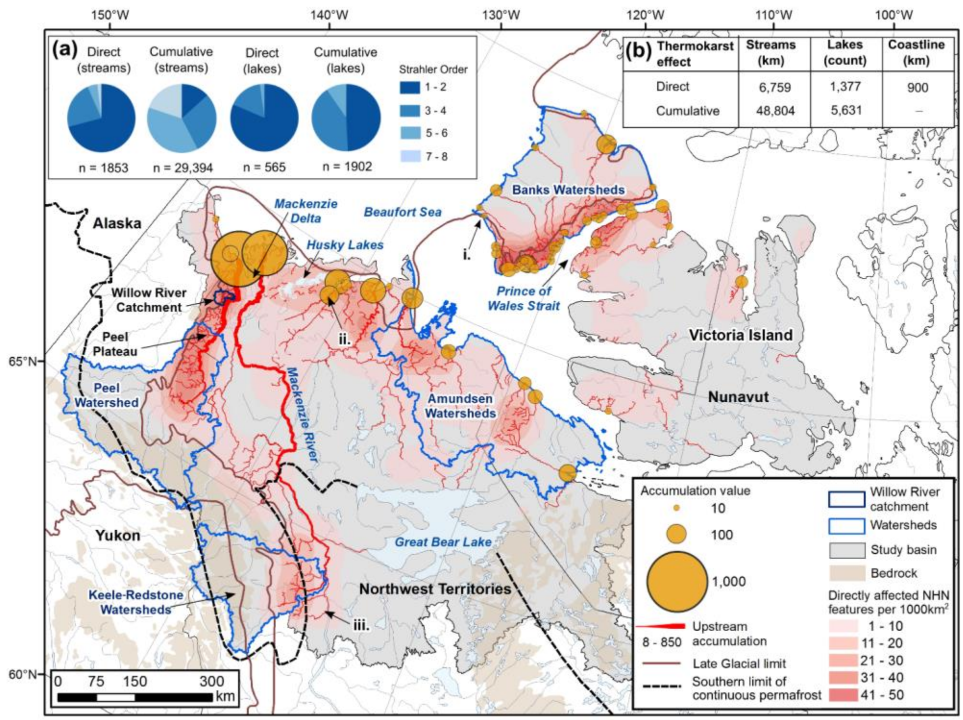

Figure 8. Thaw-driven landslide density and downstream accumulation of effects through~~,~~ ~~western Canadian~~ Arctic drainage ~~–~~from permafrost terrain of ~~from continuous permafrost terrain~~northwestern Canada. Heat map depicts all directly affected stream, lake, and coastal National Hydro Network ~~hydrological~~ (NHN) segments~~features~~ mapped. All upstream accumulation values ~~mapped~~ shown within the fluvial network are >2, and at the coast are >9. Accumulated effect contributions of the Mackenzie and Peel Rivers to the Beaufort Sea are routed separately for comparison. (a) Counts of direct and accumulated thaw-driven mass wasting effects to fluvial systems partitioned by Strahler order and hydrological feature type for ~~focal~~ the four major watersheds outlined in blue. (b) Table showing lengths of directly affected hydrological network and accumulated effects, count of directly and indirectly affected lakes and total directly affected coastline for western Arctic drainage from ~~continuous~~ permafrost terrain. Remote sensing examples of thaw-driven downstream sedimentation provided in Fig. S~~3~~4 for: i) Sachs River and Fish Lake, ii) Miner River inflow to the Husky Lakes estuary, and iii) massive deep-seated permafrost failure on Johnson River. Late glacial limit is from Dyke and Prest, 1987, bedrock geology is from Fulton, 1995, the permafrost boundary is from Brown et al., 1997, and the National Hydro Network (NHN) base data is from Natural Resources Canada, 2016. ~~Late~~

~~glacial limit is from Dyke and Prest, 1987, bedrock geology is from Fulton, 1995, and the permafrost boundary is from Brown et al., 1997.~~ Base map is from ESRI ArcGIS Online.

4 Discussion

4.1 Thresholds and connectivity between slopes and downstream environments

Results indicate that intensification of thaw-driven mass wasting is altering the Holocene-scale regime of sediment production, mobilization, and delivery in~~ the~~ ~~periglacia~~glacially~~l~~-conditioned permafrost landscapes of northwestern Canada (Figs. 2, 3, 6, 7e, S4). Hillslope-channel coupling is increasing as slope thermokarst disturbances evolve into multi-decadal, thaw-driven conveyors of fine-grained sediment and solutes to downstream environments.~~that the intensification of thaw-driven mass wasting is altering the Holocene-scale regime of sediment production, mobilization, and delivery in the periglacial landscapes of northwestern Canada (Figs. 2, 3, 6, 7e).~~ Slope morphology and sediment yields in unaffected catchments and the absence of relict valley fills suggest that over the past millennia, material redistribution associated with most slope failures was restricted to the slope system (Figs. 2a, 3a, b). Exceedance of critical thresholds controlling sediment detachment from hillslopes driven by interdependent factors of warming, precipitation, permafrost thaw and soil saturation (Lewkowicz and Way, 2019; Segal et al., 2016a; Ward-Jones et al., 2019) have instigated processes and feedbacks (Figs. 2, 3) (Kokelj et al., 2015), ~~which rapidly~~rapidly mobilizing~~e~~ materials and coupling~~e~~ slopes with hydrological systems across ~~a range of~~ many glacially-conditioned permafrost environments (Figs. 5-8). ~~Rapid evolution of hillslope-channel coupling has occurred because slope thermokarst disturbances have emerged as multi-decadal, thaw-driven conveyors of fine-grained materials to the downstream environment. Slope and channel morphology and sediment yields in catchments unaffected by active mass-wasting, and absence of relict valley fills (Figs. 2, 3, 7e) suggests that over the past millennia, the majority of slope failures have restricted material redistribution to the slope system (Figs. 3a, b). Exceedance of critical thresholds controlling sediment detachment from hillslopes driven by interdependent factors of warming, precipitation, permafrost thaw and soil saturation (Lewkowicz and Way, 2019; Segal et al., 2016a; Ward-Jones et al., 2019) have instigated processes and feedbacks (Fig. 2) (Kokelj et al., 2015), which rapidly mobilize materials and couple slopes with hydrological systems across a range of glacially-conditioned permafrost environments (Fig. 8).~~ The non-linear growth of disturbances~~ over time~~, strengthening of downstream connectivity (Figs. 2-4), and predominant impacts to low-order streams (Figs. 7c-e~~d~~, 8a) emphasizes~~s the disproportionate effect~~ that increasing disturbance size is having~~is having~~ a disproportionate effect on~~on periglacial slope evolution and~~ the magnitude and duration of downstream effects.

Recent thaw-driven mobilization of slope materials has increased ~~sediment stores~~storage in valley bottoms by several orders of magnitude, forming ~~-causing the rapid aggradation of~~large valley fills~~channel beds~~ (Figs. 2, 3), and together with the steepening and lateral displacement of channels, this supply of stored materials will amplify fluvial sediment transport for decades to centuries. Slope-to-channel ~~connectivity and downstream~~ coupling is particularly enhanced in steeply incised and confined valleys~~,~~ so that environments like the Peel Plateau have emerged as hotspots of geomorphic change and downstream effects (Figs. 6, 8) (Kokelj et al., 2013; Zolkos et al., 2018). The transition from the long-term ‘supply-limited’ norm of~~ the~~ Holocene permafrost geomorphic systems (*sensu* Carson and Kirkby, 1972; Howard, 1994)~~,~~ is striking. The change is emphasized by the unprecedented climate-driven sediment mobilization from long-frozen slopes~~geomorphic response of long-frozen permafrost slopes,~~ rapidly overloading a network of newly “under fit” streams (Figs. 2, 3, 6~~, 7e~~). Enhanced slope-channel coupling ~~and increased network connectivity are~~ is evident across the study region, h~~ (Figs. 6; S3). H~~owever, the downstream conveyance of sediment and geochemical ~~constituents~~ effects will vary (~~(Kokelj et al., 2013;~~ Shakil et al., 2020~~b~~a), because the connectivity of slope and hydrological systems are inherently sensitive to substrate ~~properties~~ and ~~behaviour of~~ geochemical ~~constituents~~properties, network configuration, stream power, physiography, permafrost conditions, and climate drivers~~ including air temperatures and precipitation regimes~~. While it is difficult to translate thousands of discrete and dynamic slope disturbances into coherent estimates of river impacts at the basin-scale, this is ~~has emerged as~~ a central challenge facing periglacial geomorphologists, biogeochemists, and aquatic ecologists in the Anthropocene.

4.2 Non-linear disturbance trajectories

~~At the slope-scale, our nested study highlights the rate and volumes of material mobilised from slope thermokarst disturbance in glacially-conditioned permafrost terrain (Kokelj et al., 2017a).~~The ~~The~~ thickness of materials mobilized by thaw-driven mass wasting ~~permafrost thawed~~ is associated with disturbance volume, and both parameters relate~~are related~~ to ~~disturbance~~ thaw-slump area via power-law relationships (Sect.~~oin~~ 3.3; Fig. 4). The area-volume model we ~~have~~ derived has coefficients closely comparable to landslide populations in temperate environments (Klar et al., 2011). These~~ nature of these~~ relationships are~~are~~ complex because permafrost, ~~geomorphic~~geomorphic, and climatic factors~~ can~~ influence the growth trajectories~~y~~ of ~~individual~~thaw-driven slope disturbances (Figs. 2, 3), producing diverse and ~~to produce d~~dynamic morphologies~~landforms~~ over~~-~~ different ~~over~~ terrains~~ with varied material and topographic properties.~~. Regardless, these relationships ~~determined in this study~~ provide a first empirical basis for estimating thaw-driven denudation as a function of disturbance area (Figs. 4, 5~~, 7a~~), and ~~better~~ should enable better approximation of the geomorphic, sedimentary, geochemical, and carbon consequences of intensifying slope disturbance regimes. Further studies are~~investigations are~~ required to determine~~etermine~~ the potential variability in area-volume relationships with landscape type, thaw-slump development stage, material properties, and different failure modes.~~ of failure.~~

~~The rapid~~Rapid increases in the area of thaw-driven slope disturbances ~~are having~~have a major~~ a significant~~ influence on terrain evolution,~~,~~ and downslope sediment and geochemical mobilization. The increasing~~The increasing~~ prominence of larger~~,~~ and ~~thus~~ proportionately deeper disturbances~~,~~ indicates greater volumetric permafrost thaw~~ing of ice-rich permafrost~~

and sediment mobilization~~ of sediment~~ than would occur~~be anticipated~~ for the equivalent, combined surface area of numerous smal~~ler~~l slumps (Fig. 4; Table 1~~, 2~~). This~~It~~ also suggests that a greater range of material types are likely to be thawed and entrained (Fig. 2). In glacigenic deposits, materials excavated from deeper in the soil stratum ~~tend to~~ have lower organic matter contents and are~~is~~ unlikely to have ~~undergone the~~ been subject to thaw-induced geochemical changes that ~~characterise~~ characterize the active layer and near-surface permafrost (Lacelle et al., 2019). Enlargement and accelerated back wasting of the slump headwall, coalescence of thaw slumps, and polycyclic behaviour (Figs. 2, 3) increase the production of saturated substrate and the probability of material evacuation from the scar zone. As the magnitude of thaw-driven slides increases, there is also ~~also~~ greater potential for ~~underlying~~ bedrock, or in ~~southern~~ discontinuous permafrost regions, unfrozen materials, to be exposed, ~~further~~ expanding the ~~trajectories~~ range of ~~of~~ geomorphic and geochemical effects~~change~~, and increasing linkages between ~~potentially linking~~ surface and subsurface flow ~~-~~paths (Walvoord and Kurylyk, 2016).

The intensification of thaw-driven mass wasting is inextricably linked ~~to the~~ with the strengthening of ~~lateral and~~ downstream connectivity (Figs. 2, 3, 4; Tables 1~~2~~, S4~~3~~). For example, as retrogressive thaw-slumps enlarge, greater volumes of material that~~,~~ vary~~ing~~ laterally and stratigraphically are ~~being~~ mobilized, mixed as a saturated slurry, and transported by a suite of mass-wasting processes to form colluvial deposits that can veneer slopes, accumulate in downstream environments, or enter larger river channels, as well as lacustrine or coastal environments (Figs. 2, 3, S1, S3, S4) (Kokelj et al., 2015; Houben et al., 2016; Ramage et al., 2018). D~~Thaw-driven d~~ebris tongue development in small streams ~~is~~ also commonly blocks~~ing~~ drainage and has caused~~ing~~ ~~debris dam~~ lakes and ponds to form at hundreds of locations (Figs. 2, S4). The rapid ~~rapid~~ intensification of thaw-driven mass wasting combined with variation in the type of landscapes being impacted, and the nature and magnitude of material mobilized, has a range of geomorphic, biogeochemical, and ecosystem implications that require study (Tank et al., 2020; Vonk et al., 2019) so that the ~~broader-scale~~ consequences ~~of accelerating slope thermokarst~~ can be predicted in an informed manner.

4.3 The river network: transfer of thermokarst erosional materials from source to sink

~~Our~~ This spatially ~~-~~nested study~~ design~~ provides several insights on the evolving nature of slope-thermokarst and the effects on hydrological networks. Firstly, acceleration of thaw-driven mass wasting is affecting thousands of first and second-order lakes and streams in ~~permafrost preserved,~~ glacially-conditioned permafrost landscapes (Fig. 8). Major sedimentary, geochemical, and ecosystem impacts upon low-order stream networks have been abrupt~~ (Kokelj et al., 2013)~~ because the ~~increasing~~ magnitude of disturbance and enhancement of~~ed~~ downstream connectivity facilitate ~~the cascade of downstream effects~~propagation through small systems with an inherently limited capacity to absorb disturbance (Figs. 7c, d). ~~Specific examples were provided where~~ Thaw-driven mass wasting ~~slope thermokarst effects to low-order streams~~ can entirely change the character of the stream reach (Figs. 2, 3, S4), the sediment and geochemical fluxes (Fig. 7e) (Kokelj et al., 2013; Shakil et al., 2020a), and the associated habitat potential (Chin et al., 2016). Secondly, the thaw-~~driven~~ mobilized sediment and geochemical ~~mobilization is~~loads conveyed through the hydrological networks are directly impacting~~,~~ or accumulating ~~to affect~~ in thousands of low-order lakes in glacially-conditioned environments (Fig. 8) that are also inherently predisposed to abrupt limnological responses (Houben et al., 2016; Kokelj et al., 2009). Thirdly, ~~the direct effects of slope~~ slope thermokarst ~~occur~~ predominantly occurs~~on hydrological systems~~ at the 10^{-1} to 10^{2} km^{2} catchment scales where~~ (Figs. 5-8).~~ the geomorphic impacts are prolific (Figs. 5-7). Through tracking changes in the size and distribution of thaw slump features within the Willow River study catchment, we estimated a two order-of-magnitude increase in thaw-driven mass wasting from 1986 to 2018 (Figs. 5a-c). Through ~~, and,~~ integrating sediment and ground ice loss, we estimated ~~a~~about an order of magnitude increase in the contribution to catchment-scale denudation~~ of slopes~~, from 0.1 mm yr^{-1} (1986-2002) to 0.~~8~~8 mm yr^{-1} for the 2002-2018 period (Figs. 5, 6). ~~Hillslopes along the margins of 4th and 5th order drainages have also shown increasing responsiveness to thaw-driven instability and lateral river erosion, resulting in direct sediment delivery to the larger streams.~~ Fourthly, fluvial networks integrate a time-transient cascade of ~~upstream~~ watershed effects, indicating that water quality, aquatic ecosystems, and fish habitat will be affected across increasingly larger river systems and coastal environments in the study domain (Fig. 8). Hillslopes along higher-order channels are also subject to the direct effects of thaw-driven landslides, resulting in cumulative sedimentary and geochemical effects on larger systems (Figs. 6, S3, S4). Unequivocal evidence that thermokarst-derived sediments, in addition to geochemical effects~~, (Kokelj et al., 2013; Tank et al 2016)~~ are propagating through fluvial networks is provided by channel re-routing and rapid infilling of a large lake where the Willow River ~~fluvial network~~ discharges to Mackenzie Delta (Fig. 6; Video S3), and by the increases in turbidity of numerous downstream lake, delta, estuary, and coastal environments (Fig~~s~~. S~~4~~2~~i-iii~~), which coincide with our predicted areas of downstream accumulated effects (Fig. 8).

4.4 Hydrological connectivity defines a significant global change hotspot

The significance of thaw-driven mass wasting~~thermokarst processes~~ is~~are~~ magnified by the propagation of sedimentary and~~,~~ geochemical~~ and ecological~~ effects to freshwater systems and the marine environment (Ramage et al., 2018; Rudy et al., 2017a; Vonk et al., 2019). While we have not simulated dynamic routing of sediment across the 1,000,000 km^{2} study area, our nested design demonstrates evolving linkages between slope thermokarst and hydrological systems (Figs. 2-~~7), and projects the potential downstream effects at the 10^6 km^2 basin scale~~ 8~~(Fig. 8~~). Rapid proliferation of numerous, major point source disturbances amplifies the potential of downstream cumulative effects as mobilized sediments, solutes, and carbon transit a sequence of storage reservoirs~~,~~ and reinforce a thermokarst signal that is projected to cascade across increasing watershed scales to marine environments through the coming century. Although this broad-scale analysis (Fig. 8) neglects relative disturbance intensity, geomorphic and biogeochemical sinks, the variation~~s~~ in slope-downstream connectivity, and transport gradients, ~~our projection~~it provides a spatially explicit framework for exploring the distribution and ~~time-transient~~ propagation of ~~slope~~ thermokarst effects through hydrological networks. Identification of ~~major~~ thaw-driven sediment and solute source areas, and the primary hydrological networks that convey slope thermokarst effects to coastal environments, emphasizes the interconnected nature of ~~a~~ this globally significant thermokarst hotspot (Fig. 8), and could guide future scientific investigations in the study region.

4.5 Glacial legacy controls intensity of ~~slope thermokarst and~~ thaw-driven mass wasting and impacts to~~reconfiguration of~~ fluvial networks

Glacial legacy, geomorphic setting, and climate history ~~all~~ combine to determine the distribution and intensity of thaw-driven mass wasting, and the nature and routing of downstream effects across~~ continuous~~ permafrost terrain of northwestern Canada (Figs. 1, 8) (Kokelj et al., 2017a). A cooling trend through the Holocene (Porter et al., 2019) ~~has~~ preserved ground ice and maintained moraine, glaciofluvial, glaciolacustrine, and glaciomarine deposits in a quasi-stable state~~.~~, though ~~C~~climate-driven episodes of permafrost thaw, most notably in the early Holocene, have left their imprint in the form of ancient landslide scars, thaw lakes, colluvial deposits, and a regional thaw-unconformity (Burn, 1997; Lacelle et al., 2019; Mann et al. 2010; Murton, 2001). However, the millennia of cold-climate constraints on slope evolution and fluvial network development are made apparent by the abundance of steeply incised, or solifluction-smoothed valley slopes underlain by ice-rich permafrost, and now juxtaposed with adjacent, increasingly ~~enormous~~ large climate-driven mass wasting features that are mobilizing ~~discordant very large volumes of materials~~large volumes of materials ~~to low-order hydrological systems~~ that far exceed ~~stream~~ the transport capacity of low-order streams (Figs. 2, 3, 5, 6, S3, S4)~~ (Kokelj et al., 2015)~~. In continuous permafrost regions, climate-driven rejuvenation of post-glacial permafrost slope evolution is driven primarily by top-down thawing causing shallow sliding and thaw slump development (Figs. 1-3~~, 2, 5, 6~~) (Lewkowicz and Way, 2019; Segal et al., 2016a; Ward-Jones et al., 2019). However, ground warming and a loss of soil strength at depth have also led to increasing frequency and magnitude of deep-seated rotational and translational slope failures in low and subarctic environments (Figs. S3, S4iii) (Aylsworth et al., 2000; Young et al., 2020). The intensification of precipitation regimes throughout parts of the study area has increased thermoerosion, shallow landsliding, and downslope sediment transfer in active thaw slumps so that thawing slopes are increasingly pushed toward an unstable state (Fig. 2) (Kokelj et al., 2015). ~~In the subarctic~~Furthermore, ecosystem disturbances such as forest fires are expected to occur more frequently in the region with climate change (Wotton et al., 2010), compound effects of ~~climate~~ warming on permafrost (Holloway et al., 2020), and can trigger~~ing~~ an array of slope mass-wasting processes in areas already predisposed to slope instability (Fig. 8). The present intensification of thaw-driven mass wasting and increasing sedimentary and geochemical fluxes could be counteracted by feedbacks such as climate cooling, exhaustion of sediment supply and progressive loss of ground ice from the most sensitive slopes, and gradual thaw-driven decrease of slope gradients, however, these processes are most relevant at centennial time-scales or greater.

The most intensive slope thermokarst activity in North America, and perhaps across the circumpolar Arctic, has been associated with western margins and recessional positions of the Laurentide ice-sheet (Figs. 1, 8) (Kokelj et al., 2017a) where preservation of relict segregated and glacier ice (Lacelle et al., 2010; Lakeman and England, 2012; Mackay, 1971; Murton et al., 2005) and aggradation of Holocene ground ice (Burn, 1997; Holland et al., 2020) is hosted within thick glacigenic deposits. These ice-rich glacial materials are derived largely from Paleozoic and Cretaceous sedimentary rocks, and the majority of the deposits include fine-grained, solute-rich materials, easily mobilized by thaw-driven slope failure ~~(Figs. 2, 3)~~ and fluvial processes (Figs. 2-3, 6, S4~~3~~) ~~(Kokelj et al., 2013, 2015; Malone et al., 2013)~~. These environments stand in contrast to the relatively stable slopes of glaciated terrain in ~~shield~~ shield-dominated landscapes ~~including~~ in~~the~~ southeastern portions of this study region. Areas of uplifted and incised glaciomarine deposits also fit within the framework of permafrost preserved glacially-conditioned landscapes, and although many are outside of our study domain, significant terrain, sedimentary, and geochemical responses to thawing slopes have been documented there (Kokelj and Lewkowicz, 1999; Ward-Jones et al., 2019).

The ~~abrupt~~ rapid intensification of ~~slope thermokarst~~thaw-driven mass wasting and the patterns of impacts across fluvial networks of northwestern Canada indicate a deglaciation-phase response pattern (Figs. 2,~~ 3,~~ 6–~~,~~ 8), which reflects a typically ~~rapid~~ abrupt period of geomorphic transition (Ballantyne, 2002), that in permafrost regions has experienced a long-term climatic hiatus through a cooling Holocene. While more data are needed to ~~fill in~~describe the full spectrum of annual fluvial sediment yield across catchment scales in thermokarst-affected landscapes, there is a consistent pattern of much higher fluxes in headwater systems, the site of ‘primary’ glacial sediment stores (*sensu* Ballantyne, 2002). This pattern in thermokarst affected permafrost regions contrasts with that found in temperate British Columbia’s post-glacial river systems, where primary glacigenic sediment stores have been exhausted: those materials have cascaded through fluvial networks over millennia and are now reworked and transported by larger rivers (>1,000 km^2; Church and Slaymaker, 1989). In glacially-conditioned permafrost landscapes, climate-driven ~~mobilization~~ thaw of ~~these~~ glacial sediment stores is ~~currently~~ overwhelming the transport capacity of low-order streams, leading to valley-filling, upstream pond and lake formation, and river aggradation that will reinforce this early-stage paraglacial signal for centuries to come. The prospect that climate~~-~~ change is ~~renewing~~ rejuvenating the sequence of post-glacial landscape evolution points to the massive potential for thermokarst-driven geomorphic change o~~n~~f ice-rich slopes, and the centennial to ~~millennial~~ millennial-scale perturbation of downstream fluvial systems (i.e., Church and Slaymaker, 1989)~~,~~ and the receiving lacustrine, deltaic, and coastal environments in several Arctic regions ~~in several Arctic regions~~ (Kokelj et al., 2017a).

5. Conclusions

Non-linear intensification of thaw-driven mass wasting is transforming permafrost preserved glacigenic landscapes and downstream connectivity, triggering a cascade of effects that are propagating through Arctic hydrological networks. In the most intensely impacted watersheds, hundred-fold increases in thaw-driven geomorphic activity have been quantified over a three-decade period. Power-law relationships between thaw slump area and volume emphasize the non-linear influence of increasing disturbance area on landscape morphology, slope to stream connectivity, and downstream effects. The disequilibrium imposed by thaw-driven release of glacigenic ~~massive~~ sediment stores from the headwater slopes (1^{st} and 2^{nd}-order streams) reflects a tipping point within these ~~long-frozen~~ permafrost land systems and signals decadal to millennial-scale~~a persistent~~ perturbation of downstream hydrological networks. ~~We can anticipate that thaw-driven mobilization of sediments and soluble materials and their cascade through western Canada's Arctic river networks will enhance connectivity, and fundamentally alter the sediment transporting characteristics of long-quiescent slopes and streams with major implications to downstream geomorphic, geochemical and ecological conditions, and compounding localized thermokarst effects to lake and coastal systems.~~

We estimate that thaw-driven mass wasting directly affects approximately 6760 km of stream segments, 1380 lakes, and 900 km of coastline across the 994,860 ~~1,000,000~~ km^2 Arctic drainage area from permafrost terrain ~~from continuous permafrost~~ ~~o~~of northwestern Canada. The propagation of thermokarst effects through fluvial networks has the potential to increase the number of affected lakes by at least a factor of 4.0~~,~~ and the length of the impacted fluvial network by a factor of 7.0. Projection of accumulated slope-thermokarst effects indicates that there are~~d~~ numerous susceptible lake, delta, estuary and coastal environments throughout the study ~~basin~~region. Major thaw-driven geomorphic activity is concentrated along ice-rich moraine systems that define coastal regions of Banks and Victoria Islands bounding Prince of Wales Strait, where numerous, small, intensely affected fluvial systems transfer thermokarst-derived sediments and solutes short distances to the coastal environment. In contrast, the thaw-driven sediment and solute loads conveyed by hundreds of upland streams draining glaciated, ice-marginal landscapes of the lower Peel and Mackenzie watersheds are routed into the two major rivers and indicate a ~~long-term~~centennial to millennial~~–~~-scale cascade of thermokarst effects to the Mackenzie Delta and the Beaufort Sea. The varying intensity of thaw-driven slope disturbances and the propagation of sedimentary and biogeochemical effects (i.e., dissolved vs. particulate; carbon vs. nutrients vs. major ions) across hydrological networks of varying configuration (e.g., channel slope, lake density, size) will define the evolution of downstream geomorphic, ecological, and biogeochemical systems over the coming centuries.

Glacially-conditioned permafrost terrain exhibits exceptionally strong climate-geomorphic linkages and massive potential for thaw-driven geomorphic transformation~~, and underlines exceptionally strong climate-geomorphic linkages~~. Intensifying slope thermokarst effects are propagated through hydrological networks,~~ greatly~~ amplifying the extent, magnitude, and duration of impacts related to permafrost thaw~~. This study highlights the interconnected nature of climate-driven thermokarst~~. ~~by quantifying relationships between intensification of disturbance and strengthening of downstream linkages, and by projecting the cascade of effects across hydrological networks to coastal systems of northwestern Canada.~~ Through placing thaw-driven geomorphic phenomena in a geological and hydrological framework, spatial patterns and trajectories of landscape change, as well as environmental consequences, can be contextualized and predicted in an informed manner. Glacial legacy, rejuvenation of post-glacial permafrost landscape evolution, and patterns of continental drainage dictate that western Arctic Canada will be an interconnected thermokarst hotspot of global significance through the coming millennia.

Data availability. Datasets used in this publication and sources are ~~The datasets are referred to in text~~summarized in Table S1. ~~and links are in the reference list.~~ Framework and geoprocessing steps for developing flow accumulation analysis are available in the Supplementary materials.

Supplementary materials. The supplement related to this article is available online at: https://tc.copernicus.org/preprints/tc-2020-218/tc-2020-218-RC2-supplement.pdf

Author contributions. SVK and JT developed the paper concept. All authors contributed to field data collection and analysis of data and refinement of paper scope. JV~~S~~ processed ~~and analysed the~~the UAV and LiDAR ~~data~~and developed statistical analyses on the datasets with input from SVK and JT. JK and SVK developed the flow network analysis with input from JT and AR. AR, JV~~S~~ and JK produced final f~~F~~igures. SVK drafted and revised the paper with input from all authors.

Competing interests. The authors declare that they have no conflict of interest.

Acknowledgements. The work has been funded by the Department of Environment and Natural Resources Climate Change and Northwest Territories Cumulative Impact Monitoring Program of the Government of the Northwest Territories, the Natural Science and Engineering Research Council of Canada, and the Polar Continental Shelf Program, Natural Resources Canada. Institutional support from the Tetl'it and Ehdiitat Renewable Resource Councils, the Inuvik, Tuktoyaktuk and Sachs Harbour Hunters and Trappers Committees, the Inuvialuit Joint Secretariat, the Inuvialuit Land Administration, the Aurora Research Institute and the NWT Centre for Geomatics have been critical to the success of this research program. Field support and logistical coordination from Christine Firth, Joel McAlister, Georgina Neyendo, Eugene Pascale, Steven Tetlitchi, Alice Wilson, and Billy Wilson are gratefully acknowledged. We would also like to acknowledge reporting of major landslide incidents from Donald Arey, Douglas Esagok, Eric McLeod and Connor Gould. Photographs in Figure 2 were provided courtesy of Rob Fraser, Canada Centre for Remote Sensing. This research has benefited from ongoing discussions with Chris Burn, Douglas Esagok, Rob Fraser, Denis Lacelle, Trevor Lantz, Steven Tetlitchi, and Stephen Wolfe. Thoughtful and detailed comments by Stephan Gruber, Julian Murton, Ingmar Nitze and handling Editor Peter Morse have improved this manuscript. This is NWT Geological Survey contribution 0138.

~~*Acknowledgements*. The work was supported by the Department of Environment and Natural Resources Climate Change and Northwest Territories Cumulative Impact Monitoring Program of the Government of the Northwest Territories, the Natural Science and Engineering Research Council of Canada, and the Polar Continental Shelf Program, Natural Resources Canada. Long-term support from the Tetl'it and Ehdiitat Renewable Resource Councils, the Inuvik, Tuktoyaktuk and Sachs Harbour Hunters and Trappers Committees, the Inuvialuit Joint Secretariat, the Inuvialuit Land Administration and from the Aurora~~

~~Research Institute and NWT Centre for Geomatics are gratefully acknowledged. Field support from Christine Firth, Eugene Pascale, Steven Tetlitchi, Alice Wilson, and Billy Wilson are gratefully acknowledged. Photographs in Figure 3 were provided courtesy of Rob Fraser, Canada Centre for Remote Sensing. This research has benefited from discussions with Chris Burn, Douglas Esagok, Rob Fraser, Denis Lacelle, Trevor Lantz, Peter Morse and Stephen Wolfe. We appreciate detailed and thoughtful Ccomments by Stephan Gruber, Julian Murton and Ingmar Nitze that have improved the manuscript.~~

References

Abbott, B. W., Jones, J. B., Godsey, S. E., Larouche, J. R., and Bowden, W. B: Patterns and persistence of hydrologic carbon and nutrient export from collapsing upland permafrost, Biogeosciences, 12, 3725–40, https://doi.org/10.5194/bg-12-3725-2015, 2015.

Aylsworth, J. M., Duk-Rodkin, A., Robertson, T., and Traynor, J. A.: Landslides of the Mackenzie Valley and adjacent mountainous and coastal regions, in: The Physical Environment of the Mackenzie Valley: A Baseline for the Assessment of Environmental Change, edited by: Dyke, L. D., and Brooks, G. R., Geological Survey of Canada Bulletin 547, 167-176, https://doi.org/10.4095/211888, 2000.

Ballantyne, C. K.: Paraglacial geomorphology, Quaternary Sci. Rev. 21, 1935–2017, https//doi.org/10.1016/S0277-3791(02)00005-7, 2002.

Balser, A. W., Jones, J. B. and Gens, R.: Timing of retrogressive thaw slump initiation in the Noatak Basin, northwest Alaska, USA J. Geophys. Res. Earth Surf. 119, 1106–20, https://doi.org/10.1002/2013JF002889, 2014.

Bater, C. W. and Coops, N. C.: Evaluating error associated with lidar-derived DEM interpolation, Computers & Geosciences, 35(2), 289-300, https://doi.org/10.1016/j.cageo.2008.09.001, 2009.

Beel, C. R., Lamoureux, S. F., and Orwin, J. F.: Fluvial response to a period of hydrometeorological change and landscape disturbance in the Canadian High Arctic, Geophys. Res. Lett., 45, https://doi.org/10.1029/2018GL079660, 2018.

Boreggio, M., Bernard, M., and Gregoretti, C.: Evaluating the Differences of Gridding Techniques for Digital Elevation Models Generation and Their Influence on the Modeling of Stony Debris Flows Routing: A Case Study From Rovina di Cancia Basin (North-Eastern Italian Alps), Frontiers in Earth Science, 6, 89, https://doi.org/10.3389/feart.2018.00089, 2018.

Bowden, W. B., Gooseff, M. N., Balser, A., Green, A., Peterson, B. J., and Bradford, J.: Sediment and nutrient delivery from thermokarst features in the foothills of the North Slope, Alaska: Potential impacts on headwater stream ecosystems, J. Geophy. Res. Earth Surf. 113, G02026, https://doi:10.1029/2007JG000470, 2008.

Brooker, A., Fraser, R. H., Olthof, I., Kokelj, S. V., and Lacelle, D.: Mapping the activity and evolution of retrogressive thaw slumps by tasselled cap trend analysis of a Landsat satellite image stack,~~.~~ Permafrost Periglac., 25 243–56, https://doi.org/10.1002/ppp.1819, 2014.

Brown, J., Ferrians, O.J., Heginbottom, J. A., and Melnikov, E. S., eds.: Circum-Arctic map of permafrost and ground-ice conditions,~~.~~ Washington, DC: U.S. Geological Survey in Cooperation with the Circum-Pacific Council for Energy and Mineral Resources. Circum-Pacific Map Series CP-45, scale 1:10,000,000, 1 sheet, https://doi.org/10.3133/cp45, 1997 (revised 2001).

Burn, C. R.: Cryostratigraphy, paleogeography, and climate change during the early Holocene warm interval, western Arctic coast, Canada,~~.~~ Can. J. Earth Sci., 34, 912-925, https://doi.org/10.1139/e17-076, 1997.

Burn, C. R. and Kokelj, S. V.: The environment and permafrost of the Mackenzie Delta area, Permafrost Periglac., 20, 83–105, https://doi.org/10.1002/ppp.655, 2009.

Bull, W. B.: Geomorphology of segmented alluvial fans in western Fresno County, California. US Government Printing Office, USGS Prof Paper 352E, https://doi.org/10.3133/pp352E, 1964.

Carson, M.A. and Kirkby, M. J.: Hillslope Form and Process,~~.~~ Cambridge University Press, New York. 476 pp, https://doi.org/10.1017/S0016756800000546, 1972.

Chin, K. S., Lento, J., Culp, J. M., Lacelle, D., and Kokelj, S. V.: Permafrost thaw and intense thermokarst activity decreases abundance of stream benthic macroinvertebrates. Glob. Change Biol., 22, 2715–2728. https://doi.org/10.1111/gcb.13225, 2016.

Chipman, M. L., Kling, G. W., Lundstrom, C. C., and Hu, F. S.: Multiple thermo-erosional episodes during the past six millennia: Implications for the response of Arctic permafrost to climate change,~~.~~ Geology, 44, 439–442. https://doi.org/10.1130/G37693.1, 2016.

Church, M. and Slaymaker, O.: Disequilibrium of Holocene sediment yield in glaciated British Columbia,~~.~~ Nature. 337, 452–454. https://doi.org/10.1038/337452a0, 1989.

Dyke, A. S. and Prest, V. K.: Late Wisconsinan and Holocene History of the Laurentide Ice Sheet,~~.~~ Géographie Physique et Quaternaire, 41, 237-263. https//:doi.org/10.7202/032681ar, 1987.

Dyke, A. S., Moore, A., and Robertson, L.: Deglaciation of North America, Geological Survey of Canada, Ottawa, ON, Canada, Open File 1574, 2003.

Fulton, R. J. (compiler): Surficial Materials of Canada—Map 1880A Government of Canada, Natural Resources Canada, Geological Survey of Canada, Terrain Sciences Division Scale, 1: 5000000, https://doi.org/10.4095/205040, 1995.

Gould, S. B., Glenn, N. F., Sankey, T. T., and McNamara, J. P.: Influence of a Dense, Low-height Shrub Species on the Accuracy of a Lidar-derived DEM,~~.~~ Photogrammetric Engineering & Remote Sensing, 5, 421-431. https://doi.org/10.14358/PERS.79.5.421, 2013.

Holland, K. M., Porter, T. J., Froese, D. G., Kokelj, S. V., and Buchanan, C.: Ice-wedge evidence of Holocene winter warming in the Canadian Arctic,~~.~~ Geophys. Res. Lett., https://.doi.org/10.1029/2020GL087942, 2020.

Holloway, J. E., Lewkowicz, A. G., Douglas, T. A., Li, X., Turetsky, M. R., Baltzer, J. L., and Jin, H.: Impact of wildfire on permafrost landscapes: A review of recent advances and future prospects,~~.~~ Permafrost Periglac., https://doi.org/10.1002/ppp.2048, 2020.

Hornby, D. D.: RivEX (Version 10.25) [Software]. Available from http://www.rivex.co.uk, ~~.~~2017.

Houben, A. J., French, T. D., Kokelj, S. V., Wang, X., Smol, J. P., and Blais, J. M.: The impacts of permafrost thaw slump events on limnological variables in upland tundra lakes, Mackenzie Delta region,~~.~~ Fundam. Appl. Limnol., 189(1), 11-35, https://doi.org/10.1127/fal/2016/0921, 2016.

Howard, A. D.: A detachment-limited model of drainage basin evolution,~~.~~ Water Resour.~~ces~~ Res~~earch.~~, 30(7), 2261-2285, https://doi.org/10.1029/94WR00757, 1994.

Klar, A. Aharonov, E. Kalderon-Asael, B., and Katz, O.: Analytical and observational relations between landslide volume and surface area,~~.~~ J. Geophys. Res., 116, F02001, https://doi.org/10.1029/2009JF001604, 2011.

Kokelj, S. V. and Lewkowicz, A. G., 1999. Salinization of permafrost terrain due to natural geomorphic disturbance, Fosheim Peninsula, Ellesmere Island,~~.~~ Arctic, 52(4), 372-385, http://doi.org/10.14430/arctic942, 1999.

Kokelj, S. V. and Jorgenson, M. T.: Advances in Thermokarst Research,~~.~~ Permafrost and Periglac., 24, 108–119, https://doi.org/10.1002/ppp.1779, 2013.

Kokelj, S. V., Zajdlik, B., and Thompson, M. S.: The impacts of thawing permafrost on the chemistry of lakes across the subarctic boreal tundra transition, Mackenzie Delta region, Canada,~~.~~ Permafrost and Periglac., 20, 185–199, https://doi.org/10.1002/ppp.641, 2009.

Kokelj, S. V., Lacelle, D., Lantz, T. C., Tunnicliffe, J., Malone, L., Clark, I. D., and Chin, K. S.: Thawing of massive ground ice in mega slumps drives increases in stream sediment and solute flux across a range of watershed scales,~~.~~ J. Geophys. Res.-Earth. 118, 681–692, https://doi.org/10.1002/jgrf.20063, 2013.

Kokelj, S. V., Tunnicliffe, J., Lacelle, D., Lantz, T. C., Chin, K. S., and Fraser, R.: Increased precipitation drives mega slump development and destabilization of ice-rich permafrost terrain, northwestern Canada, Glob. Planet. Change, 129, 56-68, https://doi.org/10.1016/j.gloplacha.2015.02.008, 2015.

Kokelj, S. V., Lantz, T. C., Tunnicliffe, J., Segal, R., and Lacelle, D.: Climate-driven thaw of permafrost preserved glacial landscapes, northwestern Canada,~~.~~ Geology, 45, 371–374, https://doi.org/10.1130/G38626.1, 2017a.

Kokelj, S. V., Tunnicliffe, J. F., and Lacelle, D.: The Peel Plateau of Northwestern Canada: An Ice-Rich Hummocky Moraine Landscape in Transition, in: Landscapes and Landforms of Western Canada, edited by: Slaymaker, O., Springer International Publishing, 109–122, http://link.springer.com/10.1007/978-3-319-44595-3_7, 2017b.

Kokelj, S. V, Palmer, M. J., Lantz, T. C., and Burn, C. R.: Ground Temperatures and Permafrost Warming from Forest to Tundra, Tuktoyaktuk Coastlands and Anderson Plain, NWT, Canada,~~.~~ Permafrost Periglac. 28, 543–551, https://doi.org/10.1002/ppp.1934, 2017c.

Kokoszka, J. and Kokelj, S. V.: 2021~~0~~. Broad-scale mapping of hydrological features affected by slope-thermokarst from arctic drainage, Northwestern Canada: Methods and Data. Northwest Territories Geological Survey, NTGS Open Report~~.~~, 2020-013~~YYY~~, ~~XX pp.,~~ In revi~~ew~~sion 2021~~0~~.

Formatted: Font: Not Italic

Formatted: Font: Not Italic

Formatted: Font: Not Italic

Formatted: Not Highlight

Formatted: Font: Not Italic

Formatted: Font: Not Italic

Formatted: Font: Not Italic

Lacelle, D., Bjornson, J., and Lauriol, B.: Climatic and geomorphic factors affecting contemporary (1950–2004) activity of retrogressive thaw slumps on the Aklavik Plateau, Richardson Mountains, NWT, Canada,~~.~~ Permafrost Periglac., 21, 1–15, https://doi.org/10.1002/ppp.666, 2010.

Lacelle, D., Brooker, A., Fraser, R. H., and Kokelj, S. V.: Geomorphology Distribution and growth of thaw slumps in the Richardson Mountains – Peel Plateau region, northwestern Canada. Geomorphology, 235, 40–51, https://doi.org/10.1016/j.geomorph.2015.01.024, 2015.

Lacelle, D., Fontaine, M., Pellerin, A., Kokelj, S. V., and Clark, I. D.: Legacy of Holocene Landscape Changes on Soil Biogeochemistry: A Perspective From Paleo-Active Layers in Northwestern Canada,~~.~~ J. Geophys. Res.- Biogeo., 124, 2662-2679, https://doi.org/10.1029/2018JG004916, 2019.

Lakeman, T. R. and England, J. H.: Paleoglaciological insights from the age and morphology of the Jesse moraine belt, western Canadian Arctic,~~.~~ Quaternary Sci. Rev., 47, 82–100, https://doi.org/10.1016/j.quascirev.2012.04.018, 2012.

Lantz, T. C. and Kokelj, S. V.: Increasing rates of retrogressive thaw slump activity in the Mackenzie Delta region, N.W.T., Canada, Geophys. Res. Lett., 35, L06502, https://doi.org/10.1029/2007GL032433, 2008.

Lantz, T. C., Gergel, S. E., and Kokelj, S. V.: Spatial heterogeneity in the shrub tundra ecotone in the Mackenzie Delta region, Northwest Territories: Implications for Arctic environmental change, Ecosystems, 13: 194–204, https://doi.org/ 10.1007/s10021-09-9310-0, 2010.

Levenstein, B., Culp, J. M., and Lento, J.: Sediment inputs from retrogressive thaw slumps drive algal biomass accumulation but not decomposition in Arctic streams, NWT, Freshw. Biol., 63, 1300–15, https://doi.org/10.1111/fwb.13158, 2018.

Lewkowicz, A. G. and Way, R. G.: Extremes of summer climate trigger thousands of thermokarst landslides in a High Arctic environment,~~.~~ Nat. Commun., 10, 1329, https://doi.org/10.1038/s41467-019-09314-7, 2019.

Littlefair, C. A., Tank, S. E., and Kokelj, S. V.: Retrogressive thaw slumps temper dissolved organic carbon delivery to streams of the Peel Plateau, NWT, Canada,~~.~~ Biogeosciences, 14, 5487–5505, https://doi.org/10.5194/bg-14-5487-2017, 2017.

Mackay, J. R.: The origin of massive icy beds in permafrost, western Arctic coast, Canada, Can. J. Earth Sci., 8, 397–422, https://doi.org/10.1139/e71-043, 1971.

Mann, D., Groves, H. P., Reanier, R. E., and Kunz, M. L.: Floodplains, permafrost, cottonwood trees and peat: What happened the last time climate warmed suddenly in arctic Alaska? Quat. Sci. Rev. 29, 3812–3830, https://doi.org/10.1016/j.quascirev.2010.09.002, 2010.

Malone, L., Lacelle, D., Kokelj, S., and Clark, I. D.: Impacts of hillslope thaw slumps on the geochemistry of permafrost catchments (Stony Creek watershed, NWT, Canada), Chem Geol., 356, 38–49, https://doi.org/10.1016/j.chemgeo.2013.07.010, 2013.

Meng, X., Currit, N., and Zhao, K.: Ground Filtering Algorithms for Airborne LiDAR Data: A Review of Critical Issues, Remote Sens., 2(3), 833-860, https://doi.org/10.3390/rs2030833, 2010.

Murton, J.: Thermokarst sediments and sedimentary structures, Tuktoyaktuk Coastlands, western Arctic Canada, Glob. Planet. Change, 28, 175–192, https://doi.org/10.1016/S0921-8181(00)00072-2, 2001.

Murton, J. B., Whiteman, C. A., Waller, R. I., Pollard, W. H., Clark, I. D., and Dallimore, S. R.: Basal ice facies and supraglacial melt-out till of the Laurentide Ice Sheet, Tuktoyaktuk Coast- lands, western Arctic Canada, Quat. Sci. Rev., 24, 681–708, https://doi.org/10.1016/j.quascirev.2004.06.008, 2005.

Natural Resources Canada.: Canada digital elevation data [dataset]. Ottawa, ON, Canada, https://open.canada.ca/data/en/dataset/7f245e4d-76c2-4caa-951a-45d1d2051333, 2015.

Natural Resources Canada.: National Hydro Network – NHN – GeoBase Series [dataset], Ottawa, ON, Canada https://open.canada.ca/data/en/dataset/a4b190fe-e090-4e6d-881e-b87956c07977, 2016.

Nitze, I., Grosse, G., Jones, B. M., Romanovsky, V. E., and Boike, J.: Remote sensing quantifies widespread abundance of permafrost region disturbances across the Arctic and Subarctic, Nat. Commun., 9, 5423, https://doi.org/10.1038/s41467-018-07663-3, 2018.

Northwest Territories Centre for Geomatics.: Northwest Territories SPOT Mosaic [dataset] http://www.geomatics.gov.nt.ca/dldsoptions.aspx, 2013.

Olefeldt, D., Goswami, S., Grosse, G., Hayes, D., Hugelius, G., Kuhry, P., McGuire, A. D., Romanovsky, V. E., Sannel, A. B. K., Schuur, E. A. G., and Turetsky, M. R.: Circumpolar distribution and carbon storage of thermokarst landscapes, Nat. Commun., 7, 13043, https://doi.org/10.1038/ncomms13043, 2016.

O'Neill, H. B., Burn, C. R., Kokelj, S. V., and Lantz, T. C.: "Warm" tundra: Atmospheric and near-surface ground temperature inversions across an alpine treeline in continuous permafrost, western Arctic, Canada, Permafrost Periglac., 26, 103– 118, https://doi.org/10.1002/ppp.1838, 2015.

O'Neill, H. B., Wolfe, S. A., and Duchesne, C.: New ground ice maps for Canada using a paleogeographic modelling approach, The Cryosphere, 13, 753-773, https://doi.org/10.5194/tc-13-753-2019, 2019.

Pollard, W. H.: Distribution and characterization of ground ice on Fosheim Peninsula, Ellesmere Island, Nunavut, in: Environmental response to climate change in the Canadian High Arctic, edited by: Garneau, M. and Alt, B. T., Geological Survey of Canada, Ottawa, ON, Canada, Bulletin 529, 207–233, 2000.

Porter, T. J., Schoenemann, S. W., Davies, L. J., Steig, E. J., Bandara, S., and Froese, D. G.: Recent summer warming in northwestern Canada exceeds the Holocene thermal maximum, Nat. Commun., 10:1631, https://doi.org/10.1038/s41467-019-09622-y, 2019.

Rampton, V. N.: Quaternary Geology of the Tuktoyaktuk Coastlands, Northwest Territories, Geological Survey of Canada, Ottawa, ON, Canada, Memoir 423, 1988.

Ramage, J. L., Irrgang, A. M., Herzschuh, U., Morgenstern, A., Couture, N., and Lantuit, H.: Terrain controls on the occurrence of coastal retrogressive thaw slumps along the Yukon coast, Canada, J. Geophys. Res.-Earth, 122, 1619–1634, https://doi.org/10.1002/2017JF004231, 2017.

Ramage, J. L., Irrgang, A. M., Morgenstern, A., and Lantuit, H.: Increasing coastal slump activity impacts the release of sediment and organic carbon into the Arctic Ocean, Biogeosciences, 15, 1483–1495, https://doi.org/10.5194/bg-15-1483-2018, 2018.

R Core Team. 2017. *R: A language and environment for statistical computing* (version 3.4.1). Vienna, Austria: R Foundation for Statistical Computing. http://www.R-project.org.

Rudy, A.C.A., and Kokelj, S.V., 2020. Inventory of retrogressive thaw slumps in the Willow River

Formatted: Font: Not Italic

watershed, mapped using 1986, 2002, and 2018 Landsat imagery, Northwest Territories Geological Survey, NWT Open Report 2020-011, 4 pages and digital data.

~~*Rudy, A. C. A. and Kokelj, S. V.: Inventory of retrogressive thaw slumps in the Willow River watershed, mapped using 1986, 2002 and 2018 Landsat imagery. Northwest Territories Geological Survey, NTGS Open Rep. 2020-YYY, XX pp., In Review 2020.*~~

Rudy, A. C. A., Lamoureux, S. F., Kokelj, S. V., Smith, I. R., and England, J. H.: Accelerating Thermokarst Transforms Ice-Cored Terrain Triggering a Downstream Cascade to the Ocean, Geophys. Res. Lett., 44, 11080–11087, https://doi.org/10.1002/2017GL074912, 2017a.

Rudy, A. C. A., Lamoureux, S. F., Treitz, P., Ewijk, K. V., Bonnaventure, P. P., and Budkewitsch, P.: Terrain Controls and Landscape-Scale Susceptibility Modelling of Active-Layer Detachments, Sabine Peninsula, Melville Island, Nunavut, Permafrost Periglac., 28(1), 79–91, https://doi.org/10.1002/ppp.1900, 2017b.

Rudy, A.C.A., Kokelj, S.V., and Kokozska, J., 2020. Inventory of retrogressive thaw slumps on the Peel Plateau and on southeastern Banks Island, Northwest Territories using 2017 Sentinel imagery, Northwest Territories Geological Survey, NWT Open Report 2020-012, 5 pages and digital data.

~~*Rudy, A. C. A., Kokelj, S. V., and Kokoszka, J.: Inventory of retrogressive thaw slumps on the Peel Plateau and on southeastern Banks Island, Northwest Territories using 2018 Sentinel imagery. Northwest Territories Geological Survey, NTGS Open Rep., 2020-YYY, XX pp., In Review 2020.*~~

Segal, R. A., Lantz, T. C., and Kokelj, S. V.: Acceleration of thaw slump activity in glaciated landscapes of the Western Canadian Arctic, Environ. Res. Lett., 11(3), 034025, https://doi.org/10.1088/1748-9326/11/3/034025, 2016a.

Segal, R.A., Kokelj, S.V., Lantz, T.C., Durkee, K., Gervais, S., Mahon, E., Snijders, M., Buysse, J., and Schwarz, S.: Broad-scale mapping of terrain impacted by retrogressive thaw slumping in Northwestern Canada, Northwest Territories Geological Survey, NWT Open Rep. 2016-008, 17 pp., 2016b.

Segal, R.A., Lantz, T.C., and Kokelj, S.V.: Inventory of active retrogressive thaw slumps on eastern Banks Island, Northwest Territories, Northwest Territories Geological Survey, NWT Open Rep., 2015-021, 8 pp., 2016c.

Segal, R.A., Lantz, T.C., and Kokelj, S.V.: Inventory of active retrogressive thaw slumps in the Peel Plateau, Northwest Territories, Northwest Territories Geological Survey, NWT Open Rep.. 2015-020, 8 pp, 2016d.

Formatted: Font: Not Italic

Formatted: Font: Not Italic

Formatted: Font: Not Italic

Formatted: Font: Not Italic

Shakil, S., Tank, S.E., Kokelj, S.V., Vonk, J.E., and Zolkos, S.: Particulate dominance of organic carbon mobilization from thaw slumps on the Peel Plateau, NT: Quantification and implications for stream systems and permafrost carbon release,~~.~~ Environ. Res. Lett., 15, 114019, https://doi.org/10.1088/1748-9326/abac36,~~Accepted~~ 2020a.

Shakil, S., Zolkos, S., Chin, K., and Tank, S.: Total suspended solids data from streams draining permafrost thaw slumps on the Peel Plateau, Northwest Territories,~~.~~ Waterloo, Canada: Canadian Cryospheric Information Network (CCIN). https://doi.org/10.21963/13181,~~.~~ 2020b.

Smith, S. L., Romanovsky, V. E., Lewkowicz, A. G., Burn, C. R., Allard, M., Clow, G. D., Yoshikawa, K., and Throop, J.: Thermal state of permafrost in North America: a contribution to the international polar year, Permafrost Periglac., 21, 117–135, https://doi.org/10.1002/ppp.690, 2010.

Smith, M. W., Carrivick, J. L., and Quincey, D. J.: Structure from motion photogrammetry in physical geography,~~.~~ Prog. Phys. Geogr. Earth Environ., 40, 247–275, https://doi.org/10.1177/0309133315615805, 2016.

St. Pierre, K. A., Zolkos, S., Shakil, S., Tank, S. E., St. Louis, V. L., and Kokelj, S. V.: Unprecedented increases in total and methyl mercury concentrations downstream of retrogressive thaw slumps in the western Canadian Arctic,~~.~~ Environmental Science & Technology, 52(24), 14099-14109, https://doi.org/10.1021/acs.est.8b05348, 2018.

Tarboton, D., G.: A new method for the determination of flow directions and contributing areas in grid digital elevation models,~~:~~ Water Resour. Res., 33, 309–319, https://doi.org/10.1029/96WR03137, 1997.

Tank, S. E., Striegl, R. G., McClelland, J. W., and Kokelj, S. V.: Multi-decadal increases in dissolved organic carbon and alkalinity flux from the Mackenzie drainage basin to the Arctic Ocean, Environ. Res. Lett., 11(5), 054015, https://doi.org/10.1088/1748-9326/11/5/054015, 2016.

Tank, S. E., Vonk, J. E., Walvoord, M. A., McClelland, J. W., Laurion, I., and Abbott, B. W.: Landscape matters: Predicting the biogeochemical effects of permafrost thaw on aquatic networks with a state factor approach,~~.~~ Permafrost Periglac., https://doi.org/10.1002/ppp.2057, 2020.

Turetsky et al.,: Carbon release through abrupt permafrost thaw~~.~~, Nature Geoscience. https://doi.org/10.1038/s41561-019-0526-0, 2020.

Thienpont, J. R., Rühland, K. M., Pisaric, M. F. J., Kokelj, S. V., Kimpe, L. E., Blais, J. M., and Smol, J. P.: Biological responses to permafrost thaw slumping in Canadian Arctic lakes~~.~~, Freshw~~ater.~~. Biol~~ogy.~~., 58 (2), 337– 353, https://doi.org/10.1111/Fwb.12061, 2013.

van der Sluijs, J., Kokelj, S., Fraser, R., Tunnicliffe, J., and Lacelle, D.: Permafrost Terrain Dynamics and Infrastructure Impacts Revealed by UAV Photogrammetry and Thermal Imaging~~.~~, Remote Sens., 10, 1734, https://doi.org/10.3390/rs10111734, 2018.

Vonk, J. E., Tank, S. E., and Walvoord, M. A.: Integrating hydrology and biogeochemistry across frozen landscapes, Nat. Commun., 10:5377, https://doi.org/10.1038/s41467-019-13361, 2019.

Walvoord, M. A. and Kurylyk, B. L.: Hydrological impacts of thawing permafrost-A review~~.~~, Vadose Zone J.~~ournal~~, 15(6), https://doi:10.2136/vzj2016.01.0010, 2016.

Ward-Jones, M. K. W., Pollard, W. H., and Jones, B. M.: Rapid initialization of retrogressive thaw slumps in the Canadian high Arctic and their response to climate and terrain factors,~~.~~ Environ. Res. Lett~~Environment Research Letters~~., 14, 055006. https://doi.org/10.1088/1748-9326/ab12fd, 2019.

West, J. J. and Plug, L. J.: Time-dependent morphology of thaw lakes and taliks in deep and shallow ground ice,~~.~~ J. Geophys. Res. – Earth. 113: F01009, https.//doi.org/10.1029/2006JF000696, 2008.

Wohl., E: Connectivity in rivers. Prog. Phys. Geog., 41(3), 345-362, https://doi.org/10.1177/0309133317714972, 2017.

Wotton, B. M., Nock, C. A., and Flannigan, M. D.: Forest fire occurrence and climate change in Canada, Int J Wildland Fire., 19, 253-271. https://doi.org/10.1071/WF09002, 2010.

Young, J. M., van der Sluijs, J., Kokelj, S.V., and Froese, D.: Recent development of deep permafrost landslides (molard-type) in discontinuous permafrost from the central Mackenzie Mountain foothills, Northwest Territories, Canada. GSA Online, 26-30 October 2020.

Zolkos, S., Tank, S. E., and Kokelj, S. V.: Mineral Weathering and the Permafrost Carbon-Climate Feedback, Geophys. Res. Lett., 45, https://doi.org/10.1029/2018GL078748, 2018.

Zolkos, S., Tank, S. E., Striegl, R. G., Kokelj, S. V., Kokoszka, J., Estop-Aragones, C., and Olefeldt, D.: Thermokarst amplifies fluvial inorganic carbon cycling and export across watershed scales on the Peel Plateau, Canada, Biogeosciences, https://doi.org/10.5194/bg-17-5163-2020, 2020.

Zwieback, S., Kokelj, S. V., Gunther, F, Boike, J., Grosse, G., and Hajnsek, I.: Sub-seasonal thaw slump mass wasting in not consistently energy limited at the landscape scale,~~.~~ The Cryosphere, 12, 549–564, https://doi.org/10.5194/tc-12-549-2018, 2018.

~~Zolkos, S., Tank, S. E., Striegl, R. G., Kokelj, S. V., Kokoszka, J., Estop-Aragones, C., and Olefeldt, D.: Thermokarst amplifies fluvial inorganic carbon cycling and export across watershed scales on the Peel Plateau, Canada. Biogeosciences https://doi.org/10.5194/bg-2020-111, In Revision, 2020.~~